Strain migration during multiphase extension, Stord Basin, northern North Sea rift

Hamed Fazlikhani[1, 2], Synne S. Aagotnes[2, 3], Marte A. Refvem[2, 4], James Hamilton-Wright[5, 6], Rebecca E. Bell[5], Haakon Fossen[2, 7], Robert L. Gawthorpe[2], Christopher A-L. Jackson[5], Atle Rotevatn[2]

[1] GeoZentrum Nordbayern, Friedrich-Alexander-Universität (FAU) Erlangen-Nürnberg, Schlossgartern 5, 91054 Erlangen, Germany

[2]Department of Earth Science, University of Bergen, PO Box 7800, 5020 Bergen, Norway

[3]Now at Petrolia NOCO AS, Espehaugen 32 B, 5258 Blomsterdalen - Norway

[4]Now at Equinor ASA, 5020 Bergen, Norway

[5]Basins Research Group (BRG), Department of Earth Science and Engineering, Imperial College, Prince Consort Road, London SW7 2BP, UK

[6]Now at BP Exploration Operating Company Limited, Chertsey Road, Sunbury-on-Thames, Middlesex, TW16 7LN, UK

[7]Natural History Collections, University of Bergen, PO Box 7800, 5020 Bergen, Norway

Abstract

In multirifted regions, rift-related strain varies along and across the basin during and between each extensional event, and the location of maximum extension often differs between rift phases. Despite having a general understanding of multiphase rift kinematics, it remains unclear why some parts of the rift are abandoned, with strain accumulating in previously less deformed areas, and how seismic and sub-seismic scale pre-existing structures influence fault and basin geometries. We study the Stord Basin, northern North Sea, a location characterized by strain migration between two rift episodes. To reveal and quantify the kinematics, we interpreted a dense grid of 2D seismic reflection profiles, produced time-structure and isochore maps, collected quantitative fault kinematic data and calculated the amount of extension (β-factor). Our results show that the locations of basin-bounding fault systems were controlled by pre-existing crustal-scale shear zones. Within the basin, rift faults mainly developed at high angles to the Permo-Triassic Rift Phase 1 (RP1) E-W extension. Rift faults control the locus of syn-RP1 deposition, whilst during the inter-rift stage, sedimentary processes (e.g. areas of clastic wedge progradation) are more important in controlling sediment thickness trends.

The calculated amount of RP1 extension (β-factor) for the Stord Basin is up to β=1.55 (±10%, 55% extension). During Middle Jurassic-Early Cretaceous (Rift Phase 2, RP2) however, strain localises to the west along the present axis of the South Viking Graben, with the Stord Basin being almost completely abandoned. Migration of rift axis during RP2 is interpreted to be related to the changes in lithospheric strength profile and possible underplating due to the ultraslow extension (<2mm/yr during RP1) and the long period of tectonic quiescence (ca. 70 myr) between RP1 and RP2. Our results highlight the very heterogeneous nature of temporal and lateral strain migration during and between extension phases within a single rift basin.

Introduction

In multirifted basins the location of maximum extension (the rift axis) often differs between rift phases. Several factors have been proposed to control rift axis migration and rift basin abandonment during later extension phases, such as variations in lithospheric and asthenospheric rheology, crustal strength profiles during extension, duration of tectonic quiescence between rift phases (interrift period), and extension rate (Tett & Sawyer; Braun, 1992; Bertotti *et al.*, 1997; van Wijk & Cloetingh, 2002; Naliboff & Buiter, 2015; Tetreault & Buiter, 2018). Role of these parameters are mainly studied using numerical forward modelling. Such multi-phase rift basins exist in Thailand (Morley, 2017) the North Falkland Basin (Bransden *et al.*, 1999), East Greenland (Rotevatn *et al.*, 2018), the northern North Sea (Badley *et al.*, 1984; Gabrielsen, R. H. *et al.*, 1990; Ziegler, 1992; Færseth, 1996), and the Mid-Norwegian margin (Lundin & Doré, 1997; Reemst & Cloetingh, 2000). Here, the northern North Sea rift basin is used as an example of a multirifted basin thanks to its well-known geological history and data availability, providing a unique opportunity to study the potential parameters causing rift axis shifting between extensional events.

The northern North Sea rift is the result of two main episodes of crustal extension; a Late Permian-Early Triassic phase (RP1) and a Middle to Late Jurassic-Early Cretaceous phase (RP2). The rift developed in rheologically and structurally heterogeneous crust, containing a range of structures inherited form the Caledonian orogeny and a subsequent extensional collapse in the Devonian (Séranne & Séguret, 1987; Fossen, 1992; Osmundsen & Andersen, 1994). The ~450 km long, NE-SW-striking, Viking–Sogn graben system roughly defines the RP2 rift axis (Fig. 1), whereas RP1 extension was somewhat more distributed (Badley *et al.*, 1988; Steel & Ryseth, 1990; Steel, 1993; Færseth, 1996; Odinsen *et al.*, 2000b; Lervik, 2006; Tomasso *et al.*, 2008; Claringbould *et al.*, 2017). The amount of crustal extension (β-factor) during RP2 is thought to be less than RP1 and mainly accommodated by large normal faults bounding the Viking and Sogn grabens (Roberts *et al.*, 1993; Roberts *et al.*, 1995;

Odinsen *et al.*, 2000b; Bell *et al.*, 2014). The main RP1 axis and related rift basins are located along the Horda Platform and East Shetland Basin on the east and west of the Viking Graben, respectively (Steel, 1993; Færseth, 1996; Lervik, 2006). Despite an improved understanding of RP1 development in the East Shetland Basin and northern Horda Platform, principally due to the availability of larger, higher-quality, 3D seismic reflection datasets (Tomasso *et al.*, 2008; Bell *et al.*, 2014; Whipp *et al.*, 2014; Duffy *et al.*, 2015; Claringbould *et al.*, 2017; Deng *et al.*, 2017a), our knowledge about the development and architecture of the Stord Basin, the main RP1 basin in northern North Sea, is very limited.

Here we use high-quality 2D seismic reflection data and 23 exploration wells to investigate temporal and spatial variations in structural styles and depositional patterns within the Stord Basin during RP1 and RP2. We also measure the ratio between cumulative fault displacement and length and compare these data with global fault databases, including faults affected by pre-existing structures (Kim & Sanderson, 2005; Paton, 2006; Deng *et al.*, 2017b). We use our observations on fault displacement vs. fault length to discuss the potential influence of subseismic and seismic scale structural inheritance on rift fault and basin geometry. Calculated extension (β-factor) across the Stord Basin during RP1 and RP2 are compared with similar estimates from other basins in the northern North Sea rift. We ultimately compare our observations form the Stord Basin with other multi-rifted basins worldwide and numerical forward models; this provides a basis for discussing the possible reasons for the observed intra-rift strain migration and the ultimate abandonment of the Stord Basin, despite it being the most extended area in the northern North Sea region during RP1.

Geological setting of the northern North Sea

The northern North Sea rift basin developed as a result of Late Permian-Early Triassic extension followed by thermal cooling and subsidence (RP1), and a Mid-Jurassic to Early Cretaceous extensional phase (RP2) followed by Cretaceous and Cenozoic, postrift thermal subsidence (Badley *et al.*, 1984; Badley *et al.*, 1988; Gabrielsen, R. H. *et al.*, 1990; Ziegler, 1990; Underhill & Partington, 1993; Færseth, 1996; Odinsen *et al.*, 2000b; Lervik, 2006). Pre-rift crystalline basement in the northern North Sea basin comprises Sveconorwegian and Lower Paleozoic rocks that experienced Caledonian orogenic deformation, followed by extensive crustal stretching in the Devonian. The basal thrust zone (décollement) reactivated as low-angle extensional shear zones (Mode I extension (Fossen, 1992). In addition, several major extensional shear zones (Nordfjord-Sogn Detachment Zone, Bergen Arc Shear Zone, Hardangerfjord Shear Zone, Karmøy Shear Zone and Stavanger Shear Zone; Fig. 1) developed during Devonian extension (Séranne & Séguret, 1987; Fossen, 1992; Osmundsen & Andersen, 1994; Vetti & Fossen, 2012). These pre-rift structures created a very (structurally and rheologically)

heterogeneous crust that was subsequently stretched. Caledonian and Devonian structures were reactivated several times in the onshore (Fossen *et al.*, 2016; Ksiensyk *et al.*, 2016) and offshore (Reeve *et al.*, 2014; Phillips *et al.*, 2016; Fazlikhani *et al.*, 2017; Lenhart *et al.*, 2019; Osagiede *et al.*, 2019) southern Norway. The Carboniferous and Permian in the North Sea area is marked by the development of post-Variscan clastics of the Rotliegend Group and evaporites of the Zechstein Supergroup, the latter being thickest in the Southern North Sea (Ziegler, 1992; Heeremans & Faleide, 2004). These evaporites extend northward into the South Viking Graben and pinch out immediately south of Stord Basin (Fig. 1).

The first rift phase (RP1) in the northern North Sea is assumed to have initiated in the late Permian and continued into the Early Triassic (Steel & Ryseth, 1990; Færseth *et al.*, 1995). The precise timing of RP1 activity is not known, since the Permian-Triassic boundary has not been penetrated by wells or dated across large parts of the northern North Sea basin. In the South Viking and Åsta grabens and the Ling Depression, where pre-RP1 units have been penetrated, RP1-related rocks overlie Zechstein Supergroup evaporites, and locally Devonian and Carboniferous sediments. At these locations, the top of the Zechstein Supergroup evaporites is defined by a high-amplitude, regionally mappable seismic reflection (Jackson & Lewis, 2013; Phillips *et al.*, 2016; Fazlikhani *et al.*, 2017). Farther north in the northern Horda Platform and East Shetland Basin, Triassic units of various ages locally overlie Caledonian crust and remnants of the Devonian basins.

The deepest RP1 basin in the northern North Sea is the Stord Basin, located on the southern Horda Platform. However, RP1 basins are also well-developed in the northern Horda Platform and in the eastern parts of the East Shetland Basin (Steel, 1993; Odinsen *et al.*, 2000b; Tomasso *et al.*, 2008; Claringbould *et al.*, 2017; Phillips *et al.*, 2019). The first rifting phase was followed by postrift thermal subsidence that lasted from the Early Triassic to Middle Jurassic, and later by Rift Phase 2 (RP2) during the Middle Jurassic to Early Cretaceous (Steel & Ryseth, 1990; Færseth *et al.*, 1995; Færseth, 1996; Odinsen *et al.*, 2000a). The deepest RP2 basins are located within and define the axes of the Viking and Sogn grabens. The amount of extension (β-factor) in the northern North Sea rift varies along and across the rift. RP1 extension is more evenly distributed across the rift compared to RP2, during which time extension was focused along the axes of the Viking and Sogn grabens (Badley *et al.*, 1988; Roberts *et al.*, 1993; Roberts *et al.*, 1995; Odinsen *et al.*, 2000b; Ter Voorde, M *et al.*, 2000). RP1 faults were reactivated or cross-cut by RP2 faults (Tomasso *et al.*, 2008; Bell *et al.*, 2014; Whipp *et al.*, 2014; Duffy *et al.*, 2015; Claringbould *et al.*, 2017; Deng *et al.*, 2017a). However, in the Stord Basin, despite being located within the relatively well-studied, data-rich North Sea basin, the magnitude of extension and the distribution of syn-rift depocentres during RP1 and RP2 are poorly constrained.

Data and Methods

In this study we use a dense (2-3 km spacing) grid of ~ 250 regional 2D seismic reflection profiles (NSR-03/12 and SBGS-R94, courtesy of TGS, GNSR-91 and CNST86, courtesy of The Norwegian Petroleum Directorate) and 23 exploration wells in the Stord Basin (Figs. 1 and 2A). Seismic reflection profiles have variable trends and most image to depths of 9 seconds TWT (two-way time; ~20-25km) providing imaging of the middle and upper continental crust and its sedimentary cover (Fig. 2C). Formation tops from exploration wells were tied to the seismic grid using well checkshot data (Figs. 2 and 3). Eight wells located on the Utsira High and in the southeastern part of the study area encounter basement rocks (Fig. 2A). This information is used to identify and map the boundary between sedimentary cover and crystalline basement. Away from the basement-penetrating wells, our top basement interpretation (Base Rift surface) is defined as a relatively high-amplitude, laterally continuous packages of reflections that separate semi-continuous and sub-parallel reflections defining the sedimentary fill of the Northern North Sea and the more chaotic and weaker underlying reflections that characterize the crystalline basement (See Fig. 4 in Fazlikhani *et al.*, 2017 for a detailed description).

The oldest mapped seismic horizon penetrated by a borehole defines the top of the Upper Triassic (Top Hegre Group); no wells penetrate the Permian-Triassic boundary in the Stord Basin. However, on the nearby Utsira High, well 25/11-28 encountered a 345 m-thick interval of Permian Rotliegend Group below only 82 m of Triassic Hegre Group rocks. Since the Middle Triassic and older rocks have not been encountered in wells within the study area, seismic horizon interpretations older than the Upper Triassic Top Hegre Group are based on recognition of major changes in seismic facies and reflection terminations. This allows us to divide the Base RP1 to Upper Triassic Top Hegre Group into three seismic units separated by Intra syn-RP1, and Top syn-RP1 horizons (Figs. 2C and 3). We mapped four seismic horizons between the top Upper Triassic and the seabed: 1) Aalenian-Bajocian, Early Middle Jurassic (Base Brent Group), marking the Base RP2; 2) Base Cretaceous Unconformity (BCU) marking the transition from syn to post-RP2; 3) Top Lower Cretaceous (Top Cromer Knoll Group), as top of early post-RP2 and 4) Top Upper Cretaceous (Top Shetland Group), top of late post-RP2 (Figs. 2 and 3). These horizons thereby define pre-, syn, and post-RP2 units.

Time-thickness maps (isochrons) between key horizons primarily reveal fault-controlled changes in sediment thickness. An absence of fault-related thickness changes defines periods and/or locations of fault inactivity, thus by measuring the lengths of fault-bound, rift-related depocentres, we can define the active, at-surface trace-lengths of the bounding faults (Petersen *et al.*, 1992; McLeod *et al.*, 2000;

Childs *et al.*, 2003). The accuracy with which we can measure active fault length is defined by the spatial resolution of our seismic data, which we estimate to be ~25 m.

Fault kinematic analysis and rift extension estimation (β-factor)

Fault throw was constrained by measuring the vertical distance between hanging wall and footwall cutoffs of the Base syn-rift seismic horizons along rift faults. Fault throw data were collected perpendicular to fault strike using the available 2D seismic reflection lines and by creating synthetic sections where we lacked truly fault-perpendicular 2D seismic lines. Synthetic sections do not contain geophysical data (i.e. a seismic reflection image), but they do show projections of created surfaces based on the interpreted 2D seismic grid (Appendix 1).

Here, top acoustic basement is defined as the “Base RP1” and the Middle Jurassic Base Brent Group as “Base RP2”. Where fault-related folds (drag folds) are observed, the regional surface trend is extrapolated into the fault surface before throw values were measured to remove the effects of ductile deformation (i.e. 'continuous deformation'; Walsh & Watterson, 1991; Long & Imber, 2010). In order to distinguish between fault throw accrued during RP1 and RP2, we subtracted throw values measured at Base RP2 from throw values measured at base RP1 surface (throw backstripping; e.g. Veen & Kleinspehn, 2000). Throw values were first measured in time (ms, TWT) and then depth converted using available velocity-depth information (checkshot data) from exploration wells (see Fig. 3 in Fazlikhani *et al.*, 2017). Fault throw data were plotted on throw vs. length plots, from which the temporal and spatial development of rift faults were interpreted (see e.g. Peacock & Sanderson, 1991; Jackson & Rotevatn, 2013). It should be noted that when a fault consists of multiple overlapping segments (e.g. UEF3 or F2), we measure the total throw by summing throw for each segment (Appendix 1). Horizontal fault offset (heave) values were also collected and used to estimate the amount of extension (β-factor, McKenzie, 1978) during both rifting phases. We summed backstripped fault heaves across both the Base RP1 and Base RP2 surfaces to calculate pre-rift (T_o) and post rift (T_1) length along two transects; this allowed us to estimate total extension (β-factor). By combining time-thickness maps and throw-distance plots, and by estimating the amount of extension, we explore the tectono-stratigraphic development of the Stord Basin.

Structural and stratigraphic framework of the Stord Basin

In the following we describe the structural patterns and seismic-stratigraphic units related to RP1 and RP2. The main basin-bounding faults are the Øygarden Fault System (ØFS) to the east and the Utsira East Fault to the west (Figs. 1 and 2). The ØFS comprises four segments (ØFS2 – ØFS5) and is ca. 200

196 km long. The northernmost segment (ØFS1) continues northward into the northern Horda Platform
197 and is only partially imaged in the study area (Fig. 1, see Bell *et al.*, 2014). The Utsira East Fault consists
198 of five main segments (UEF1-5) and is ca. 100 km long (Figs.1 and 2).

199

200 **1) Pre-Permian basement (Pre-rift) in the Stord Basin**

201 Caledonian nappe units are drilled offshore in the Stavanger Platform in the southeast portion of the
202 study area and on the Utsira High in the western portion (Slagstad *et al.*, 2011; Riber *et al.*, 2015;
203 Fazlikhani *et al.*, 2017). Toward the southeastern edge of the Utsira High, well 25/12-1 (Fig. 2A) drilled
204 through conglomerates and sandstones of possible Devonian age (see Slagstad *et al.*, 2011).

205 The top pre-rift basement (Base Rift horizon) typically appears as a high-amplitude, largely continuous
206 reflection separating mostly continuous and sub-parallel reflections above from chaotic and
207 discontinuous, intrabasement reflections below (Fig. 3). These chaotic and discontinuous reflections
208 are interpreted as Caledonian nappes and/or Devonian rocks (seismic facies 2 in Fazlikhani *et al.*,
209 2017). High-amplitude and dipping reflections below the Base Rift horizon (seismic facies 3 in
210 (Fazlikhani *et al.*, 2017) are interpreted as shear zones with normal displacement that developed
211 during the collapse of the Caledonian orogenic lithosphere in the Devonian (Fossen, 1992; Fossen &
212 Hurich, 2005). Two of these shear zones, the Hardangerfjord Shear Zone (HSZ) and Utsira Shear Zone
213 (USZ), are located in the eastern and western portions of the study area, respectively (Fig. 2A).

214 **2) Permo-Triassic rifting (Rift Phase 1, RP1)**

215 **a) Syn-RP1**

216 Sediments between the Upper Triassic Top Hegre Group surface and Base Rift surface (Fig. 3 and
217 Appendix 2) are assigned to the Permo-Triassic rift phase (RP1). This unit is subdivided into syn- and
218 post-rift units based on lateral thickness changes observed in seismic reflection data (Fig. 2C). Intra
219 syn-RP1 and Top syn-RP1 (Early Triassic?) surfaces divide the syn-RP1 sediments into the "Early syn-
220 RP1" and "Late syn-RP1" units (Figs. 2C and 3).

221 The early syn-RP1 depocentres are bound by several rift-related faults distributed across the Stord
222 Basin (Fig. 4A). In the west, the main depocentres are located in the hanging wall of Utsira East Fault
223 segments 1 and 3 (UEF1 & UEF3, Fig. 4A) and are up to 1500 ms thick [up to 4600 m]. In the centre of
224 the Stord Basin, Faults 4 and 2 (F4 and F2) bound two ca. 1000 ms [ca. 3400 m] thick depocentres of
225 early syn-RP1 sediments (F2 and F4, Fig. 4A). In the east, a depocentre bound to the east by Øygarden
226 Fault System segment 3 (ØFS3) contains up to 1090 ms [~3000 m] of early syn-RP1 sediments, whereas
227 this unit thins northwards to only 810 ms [~2300 m] thick in the hanging wall of Fault 1 (F1, Fig. 4A).

Syn-RP1 sequences in the Stord Basin comprise Early Triassic fluvial sandstones (Steel & Ryseth, 1990; Steel, 1993; Færseth, 1996; Lervik, 2006). Since no wells in the basin have encountered Permian sediments (Rotliegend Group and/or Zechstein Supergroup), it is not possible to differentiate between Permian and early Triassic clastics from seismic reflection data alone. Zechstein evaporites were drilled south and west of the Stord Basin in the Åsta Graben, Ling Depression, and Sele and Utsira highs (west and south), and the South Viking Graben (Fig. 1, see the limit of Zechstein Supergroup). However, in the study area, wells 16/3-2, 16/3-4, 16/3-6, 16/6-1, 17/3-1; 25/6-1 and 25/12-1 penetrated basement without encountering any Permian rocks: only wells 16/3-7, 25/11-17 and 25/11-28 drilled through possible Permian clastics (Rotliegend Group) and carbonates (Zechstein Supergroup, Fig. 2A).

Away from wells, the distinctive signature of evaporites in seismic reflection data helps us identify the presence of these rocks. However, the presence or absence of Permian clastic rocks in the Stord Basin remains unclear. Toward the southern margin of the south Permian Basin (Franconian and Kraichgau Basins, SW and S Germany), Zechstein rocks consist of proximal conglomerates and sandstones that gradually become more evaporitic towards northern Germany (towards the centre of southern Permian Basin; Kiersnowski *et al.*, 1995). The absence of Zechstein evaporites in the Stord Basin might be due to the location of the basin at the northern margin of the northern Permian Basin in the vicinity of a local sediment source, similar to the Franconian and Kraichgau Basins along the southern margin of southern Permian Basin. In both cases, towards the centre of the Permian Basin, evaporites are more abundant. A lack of Permian rocks in deep wells and apparent lack of Zechstein evaporites as evaluated from seismic reflection data suggest the Stord Basin was most likely isolated during RP1, disconnected from the Ling Depression and Åsta Graben in the south, and from the South Viking Graben to the west. The apparent lack of early syn-rift deposits south of the Stord Basin (see time-thickness map in Fig. 4A) supports this hypothesis. Towards the north, however, the Stord Basin was most likely connected to the northern Horda Platform and north Viking Graben via the hanging wall of F1 (Figs. 4A and B).

Major late syn-RP1 depocentres are located in the hanging wall of ØFS3 to the east and UEF1 to the west. In the centre of the Stord Basin most of the accommodation in the hanging wall of F2, F3 and F4 was filled during early syn-RP1 and the late syn-RP1 sediment thickness is only up to 1 km (in comparison to 3.4 km during early syn-RP1; Figs. 4A and B). During late syn-RP1, only the depocentre in the hanging wall of ØFS5 expands laterally (Fig. 4B). Major faults that were active during the early syn-RP1 period remained active during late syn-RP1; only UEF5 newly initiated during the late syn-RP1 (Figs. 4A and B). The majority of faults located in the middle, northern and western parts of the basin (F1, F2, F3, F4, ØFS2, UEF3 and UEF4) have shorter apparent trace-lengths in late syn-RP2 compared to early syn-RP1; only UEF1 maintained its length, whereas UEF2 is anomalous in that it doubled in

length by lateral tip propagation. In contrast, faults in the eastern Stord basin (ØFS3, ØFS4 and ØFS5) grow laterally during late syn-RP1, expect for ØFS2 in which fault throw decreases (Figs. 4B and 5).

b) Post-RP1

The post-RP1 section is subdivided into "Early post-RP1" and "Late post-RP1". Early post-RP1 is bounded by the Top syn-RP1 (Early Triassic?) surface below and Top Hegre Group surface above, whereas the Late post-RP1 is bounded by Top Hegre Group surface below and the Base Brent Group surface above (Figs. 2C and 3). During early post-RP1, three main sediment depocentres are located in the hanging wall of F1, the northern portion of ØFS3, and in the hanging wall of UEF3 (Fig. 6A). The early post-RP1 section thins in the southern part of the basin where the interval is only up to 600 m thick in the hanging wall of UEF5 (Fig. 6A). Along the ØFS the early post-RP1 section shows significant thickness variations, from 1900 m in the northern part of ØFS3, thinning by up to 500 m southward. In general, Early post-RP1 sediments (? Early-Middle Triassic to Upper Triassic) are relatively evenly distributed through the basin compared to early and late syn-RP1 (compare Figs. 4A and 4B with Fig. 6A); this is related to the cessation of activity on several faults located in the centre of the basin (e.g. F3). Note that NE-dipping faults in the footwall of ØFS5 are outside the study area and are not discussed here (Fig. 6A).

During late post-RP1, the key sediment depocentre, which is 700 m thick (in comparison to a 2200 m thick early post-RP1 depocentre) is located in the hanging wall of UEF2 and UEF3 in the western margin of the basin (Fig. 6B). This shows a general westward shifting of the main depocentre from Early post-RP1 to Late post-RP1 (Figs. 6A and 6B). Overall, this period is marked by limited thickness variations in the basin in comparison to Early post-RP1.

Comparison of Early and Late post-RP1 time-thickness maps show that the active parts of all active faults are shorter during Late post-RP1 (Figs. 5, 6A and 6B). In the north and northeast areas, F1 and the majority of ØFS3 are no longer active (Figs. 6A and 6B). Main fault activity during early post-RP1 occurs along F1 in the north, eastern ØFS and western UEF basin bounding faults that migrates mainly to the west along UEF during late post-RP1 (Figs. 6A and 6B). Here it appears that early to late post-RP1 depocentre migration i.e. from the north-northeast to west, is synchronous with migration of rift fault activity, unlike the diachronous fault activity and rift depocentre migration during syn-RP1 (Figs. 6A and 6B).

3) Middle Jurassic – to Early Cretaceous rifting (Rift Phase 2, RP2)

a) Syn-RP2

Syn-RP2 units are bounded by the Base Brent Group (Base Middle Jurassic) and the Base Cretaceous Unconformity (BCU) surfaces (Appendix 2). The main depocentre is located in the centre of the basin, where the related succession is up to 1500 m [820 ms] thick (Fig. 7A). This depocentre is not located in the immediate hanging wall of any fault and is associated with a set of westward-prograding clinoforms known as the Hardangerfjord Delta (Gabrielsen, R. H. *et al.*, 2001; Sømme *et al.*, 2013; Jarsve *et al.*, 2014). Faults that were active during syn-RP2 are located at the eastern (ØFS3, 4, 5 and F3) and western (UEF2, 3, 4 and 5) basin margins (Fig. 7A). ØFS3 was the longest active fault during this period (ca. 74 km, Fig. 5), yet it accumulated only ca. 110 ms (~200 m) of throw (Middle Jurassic, Fig. 8).

In the central part of the basin, F3 was active during syn-RP2, with an active length of ca. 20 km (Fig. 7A), after its last activity during the Late syn-RP1. The fact that the thickest part of Hardangerfjord delta is located in the hanging wall of F3 (Fig. 8) and that F3, in addition to a relatively small portion of ØFS5, are the only faults reactivated after the ~70 myr period of inactivity between Late syn-RP1 (?Early Triassic) and syn-RP2 (Middle Jurassic), together suggest that the reactivation of F3 might be triggered by differential sedimentary loading (Fazlikhani & Back, 2015) associated with westward progradation of the Hardangerfjord delta. However, a combination of sedimentary loading and crustal extension during syn-RP2 might also explain the reactivation of F3. The time-thickness map of syn-RP2 (Fig. 7A) shows that the Stord Basin was tectonically quiescent during RP2, with only minor fault activity occurring during the earliest stages of rifting (Figs. 7A and 8).

b) Post-RP2

The Post-RP2 phase in the Stord Basin spans the Early Cretaceous to present. The Cretaceous post-RP2 deposits are here subdivided into the Lower and Upper Cretaceous, whereas the Cenozoic post-RP2 is outside the scope of this study and is not discussed further. The Lower Cretaceous sequence is bounded by the BCU below and Top Cromer Knoll Group (top Lower Cretaceous, Appendix. 2) above. The main sediment depocentre during this period is located in the northern part of the study area (Fig. 7B), reaching a thickness of up to 1000 m. A thick section also exists at the southern end of the study area (Fig. 7B). Sediment deposition therefore appears to be directed to underfilled accommodation around the edge of the previously deposited Hardangerfjord delta (dashed white line in Fig. 7B; also see Fig. 8C). No fault activity is documented in the Stord Basin during the Early Cretaceous post-RP2 period (Fig. 7B). The Upper Cretaceous sequence is marked by an evenly distributed sediment thickness throughout the basin (Fig. 7C). In the centre of the basin the Upper Cretaceous section is only up to 280 m thick, gradually increasing towards the southeast. Like the underlying Lower

Cretaceous succession, the Upper Cretaceous succession is virtually unaffected by faulting (Figs. 7C and 8).

Fault kinematics

Results of measured vertical displacement (throw) along basin bounding faults (Øygarden Fault System, ØFS) and Utsira East Fault, UEF) and four main intra-basin faults (F1-F4) in the Stord Basin are presented below. Throw values in time were measured perpendicular to the fault strike and after depth conversion are throw backstripped revealing the amount of fault throw in meters for RP1 and RP2 (Appendix 2).

a) Øygarden Fault System

The Øygarden Fault System (ØFS) consists of four major segments and bounds the eastern margin of the Stord Basin. ØFS1 extends northwards to the northern Horda Platform and is not considered further in this work (see Bell *et al.*, 2014; Whipp *et al.*, 2014). ØFS2 is the only segment that dips to the east and it is not linked to any other segments of the ØFS. This is consistent with the throw profile as measured across the Base RP1 horizon, which shows a maximum throw of 700 m in the centre, decreasing laterally towards the fault tips (Fig. 9). ØFS2 was only active during syn-RP1 (Figs 4 and 9). Throw along ØFS3 is greatest in the north (ca. 3200 m) and decreases gradually to the south (to ca. 1000 m) where it links with ØFS4 (Fig. 9). ØFS3 strikes N-S in the north but rotates NNE-SSW close to its southern tip (Figs. 2A and 9). This fault segment was mostly active during RP1, whereas some portions of this fault segment were also active during RP2 (Figs. 8A and 9). However, <200 m of throw accumulated on ØFS3 during RP2, accounting for only ca. 6% of its total offset (Fig. 9). Nevertheless, the active length of ØFS3 during RP2 reduced by ca. 18% in compare to RP1 (Fig. 9).

ØFS4 is >45 km long, striking N-S in the north and NE-SW in the south (Fig. 9). This fault segment accumulated ca. 2300 m of throw during RP1 close to the linkage point with ØFS3, with throw progressively decreasing southwards (Fig. 9). During RP2, ØFS4 accumulated ca. 200 m of throw, with throw being rather evenly distributed along the structure. Its length remains relatively constant during RP2, having reached its maximum length during late syn-RP1 (Fig. 9). Accrued throw during RP2 is <10% of that accumulated during RP1, whereas the fault length reduced by only ca. 25% (Fig. 9).

The 60 km-long ØFS5 segment strikes N-S in the north and NE-SW to the south, with a similar map view geometry to ØFS4 (Fig. 9). Maximum throw along ØFS5 is ca. 1400 m, with most of this achieved during RP1 (Fig. 9). Unlike ØFS3 and ØFS4, where maximum throw occurs close to their northern tip, the maximum throw on ØFS5 occurs close to its centre. During RP2, two isolated portions of ØFS5

were active; this contrasts with ØFS3 and ØFS4, which were seemingly active along their entire trace-lengths (Fig. 9). Throw accumulated on ØFS5 during RP2 reached ca. 150 m and ca. 100 m in the northern and southern portions of the fault, respectively. The maximum fault length was established during RP1 and this was maintained during the post-RP1 phase. However, fault length decreased to ca. 40% of its original length during syn-RP2 (Fig. 9).

b) Utsira East Fault

UEF1was only active during syn-RP1 (Figs. 4A, 4B and 5B), during which time it accumulated a maximum throw of ca. 1800 m. UEF2 has a concave-into-the-hangingwall plan-view trace, dips to the east, and is ca. 45 km long (Fig. 9). Throw on this segment increases southwards and reaches a maximum throw of ca. 2600 m close to its southern tip (Fig. 9). UEF2 is active throughout syn- and post-RP1, and also syn-RP2, although only ca. 50% of its previously established fault length was reactivated during the latter phase (Fig. 9). During RP2, UEF2 accumulated only ca. 10% of the throw accumulated during RP1.

UEF3 is concave in map view and consists of at least three east-dipping segments (Figs. 2A and 9). This structure is ca. 50 km long and accumulated up to 2800 m of throw during RP1 (Fig. 9). During RP2, UEF3 only accumulated a further ca. 280 m of throw, which is only 10% of that accumulated during RP1. During RP1 fault throw was distributed evenly along the structure, with a sharp decrease at the linkage points with neighbouring segments. UEF4 is >30 km long, with the northern portion dipping to the ESE and the southern portion to the ENE (Fig. 9). Approximately 1500 m of throw accrued on the northern portion of UEF4 during RP1, close to the linkage point to UEF3. Throw gradually decreases southwards from this point. The maximum fault length established during early syn-RP1 decreased by ca. 60% during Late syn-RP1, and then remained constant (Fig. 5B). During RP2, only the southern portion of UEF4 was active, with up to ca. 250 m of throw accumulating on a ca. 10 km long portion of the fault (Fig. 9). UEF5 is 35 km long and dips to the northeast (Fig. 9). Maximum throw along this fault segment (ca. 800 m) occurs in the centre, decreasing laterally towards the fault tips. During RP2, accumulated throw is only ca. 60% of that accrued during RP1, reaching a maximum of 300 m.

c) Intra-basin faults

We focus on four major faults in the centre of the Stord Basin (F1, F2, F3 and F4, Fig. 9). These faults have been chosen as they have a significant influence the internal basin architecture and depositional patterns. Fault 1 (F1) is a segmented fault with an overall eastward dip (Figs. 2A and 9), whereas the

northern tip of this fault (~12 km) extends beyond the study area (Fig. 1). Within the study area, F1 is about 70 km long and it was only active during the RP1, during which time it accumulated a maximum throw of ca. 1700 m (Fig. 9). The fault achieved its near-final length during early syn-RP1, before the active trace-length apparently decreased during late syn-RP1 (Fig. 5). The active fault length during early post-RP1 was ca. 30 km (Fig. 5C). F2 is located in the hanging wall of ØFS3, strikes N-S, is ca. 50 km long, and has an overall westward dip (Fig. 9). F2 was active only during syn-RP1 (Figs. 4A and 4B), during which time is accumulated ca. 1400 m of throw near its centre (Fig. 9). F3 dips to the east and is ca. 37 km long. Maximum throw on F3 during syn-RP1 was ca. 1300 m, decreasing to ca. 100 m during syn-RP2. This fault was active during early and late syn-RP1, before being reactivated during syn-RP2 along ca. 20 km of the initial fault length established during RP1 (Figs. 7A and 9). The maximum syn-RP2 fault throw is ca. 90% less than the fault throw accumulated during RP1, while the active part of the fault was only ca. 45% shorter during RP2. Such a faster fault throw decrease in comparison to fault length shortening occurred during RP2 has also been observed for ØFS and UEF fault segments. F3 is the only fault that reactivates during RP2, whereas all other faults either die out after RP1 or are continuously active during syn and post-RP1, and onwards into syn-RP2 (Fig. 5). F4 is 32 km long and dips broadly south-eastwards (Fig. 9). This fault accumulated ca. 1100 m of throw during the RP1 before becoming inactive (Figs. 4A and 4B).

Extension estimate (β factor) across the Stord Basin

The amount of rift-related extension is estimated by summing fault heaves along two E-W profiles across the Stord Basin (see Fig. 9 for the location of profiles). We sum horizontal distances between footwall and hanging wall cutoffs across interpreted seismic-scale faults for the Base RP1 and Base RP2 surfaces (top acoustic basement is taken as Base RP1 and Base Middle Jurassic surface as Base RP2). The difference between the present and restored length of the Base RP2 horizon is the extension for the second phase of rifting, while the difference in length between the present and restored RP1 horizon gives the extension for the full rift history. An important consideration in measuring crustal extension by heave summation is the contribution of sub-seismic faulting, which is typically estimated to 20-40% of the total extension for our level of seismic resolution. The resolution relevant here is the lower limit of fault sizes detectable from our seismic data, which we estimate to be ca. 40 m at 500 ms depth, increasing to ca. 60 m at 5000 ms depth (Walsh *et al.*, 1991; Marrett & Allmendinger, 1992; Morley, 1996). Another source of error relates to fault block rotation (Sclater & Célérier, 1988) and the amount of erosion on the fault footwall block, particularly on large-displacement, basin-bounding faults such as ØFS and UEF (Morley, 1996). However, block rotations are limited in the study area, and

footwalls appear more or less uneroded. We therefore only consider the additional contribution from subseismic faults to be significant.

Measured RP1 crustal extension along the two profiles shown in Fig. 9 gives a stretching factor (β) of 1.39 (23.3 km of extension) in the north of the basin and β=1.22 (11.2 km of extension) in the south (Table 1). Accounting for subseismic faulting (30% ± 10% of total extension) gives β=1.55 (33.3 km of extension) and β=1.32 (16 km of extension) for the northern and southern areas, respectively. Extension is significantly lower during RP2 in the Stord Basin, with β=1.009 (750 m of extension) in the north and β=1.004 (230 m of extension) in the south (Table 1). Accounting for subseismic faulting (30% ±10% of total extension) gives β=1.013 (1.07 km of extension) and β=1.006 (0.36 km of extension) for the northern and southern areas, respectively. Comparing the northern and southern part of the Stord Basin reveals that ca. 48% more extension occurred during RP1 (considering the 30% ± 10% adjustment for sub-seismic deformation) in the north. The RP2 extension is 33% more in the north. These results show that the Stord basin mainly developed during RP1, with ca. 95% of total extension (accumulated during RP1, RP2 and interrift period) occurring during this time, and that the area experienced largely tectonic quiescence during RP2.

Discussion

Regional perspectives of crustal stretching

Previous estimates of RP1 and RP2 extension in the northern North Sea have been calculated using several different methods, including crustal-scale thickness and subsidence backstripping. Klemperer (1988) provide a present-day crustal thickness map for the northern North Sea basin, showing that the crustal thickness along the northern and central Viking Graben is <16 km, and <21 km along the southern Viking Graben (T_1, post-rift crustal thickness). This value increases towards the eastern and western rift margins to ca. 26 km (See Fig. 8b in Klemperer, 1988). Sources of error for these crustal thickness estimates are related to the depth to Moho, basement velocity, the distribution and the thickness of the Palaeozoic sedimentary section, and the interpretation of the Base Triassic horizon. Assuming a pre-rift crustal thickness (T_o) of 35 km and a simple pure-shear style ductile deformation of the crust, the total amount of rift-related crustal extension under the north Viking Graben is β=2.18, β=1.66 and β=1.34 for present crustal thicknesses of 16, 21 and 26 km (T_1) respectively (Fig. 10). These estimates of crustal stretching are for the complete Late Paleozoic-Mesozoic rift; the RP1 and RP2 are not differentiated.

Syn-rift forward modelling and postrift flexural backstripping along two sections on the Horda Platform and on the East Shetland Basin suggest β=1.4 for the northern Horda Platform and β=1.15

for the East Shetland Basin during RP1 (Fig. 10, Roberts *et al.*, 1993; Roberts *et al.*, 1995). The same studies estimate β=1.05 for the northern Horda Platform, β=1.3-1.4 for the northern Viking Graben, and β=1.15 for the East Shetland Basin during RP2. Odinsen *et al.*, 2000b applied crustal-scale forward modelling with an initial uniform crustal thickness of 35 km to produce an estimate of β=1.33 for RP1 in the northern Horda Platform, β=1.41 for the northern Viking Graben, β=1.29 for the eastern East Shetland Basin and β=1.14 for the western East Shetland Basin (Fig. 10). Overall stretching factor estimations by Roberts *et al.*, 1993; Roberts *et al.*, 1995 and Odinsen *et al.*, 2000b are in good agreement and are slightly higher than the values calculated by fault heave summation by Bell *et al.*, 2014 in the northern Horda Platform and Måløy Slope (Fig. 10). Stretching factor estimates for the northern Horda Platform are <β=1.4, which is below a proposed minimum value of β=1.5 for the initiation of partial melting and underplating of the crust (Foucher *et al.*, 1982; McKenzie & O'Nions, 1991). However, Wrona *et al.*, 2019 have identified potentially large volumes (472 ± 161 km^3) of now-crystallized lower crustal melt below this region. In the Oslo Rift and its equivalent offshore Skagerak Rift, crustal partial melting occurred with crustal stretching estimates of β =1.4-1.6 (Ro & Faleide, 1992).

Considering previous estimates of crustal stretching, our results indicate that in the southern Horda Platform, the Stord Basin experienced larger amounts of extension during RP1 (β=1.55 ±10% in the basin centre) than the northern Horda Platform (β =1.26-1.4). In southern Norway, directly east of the Stord Basin, Permo-Triassic igneous dykes occur (Fossen & Dunlap, 1999). The likely presence of magmatic intrusions beneath the northern Horda platform (Wrona et al., 2019), despite the area experiencing less extension during RP1 than the Stord Basin, and the presence of dykes onshore southern Norway suggest that melting and magmatism might have occurred in the deeper parts of the Stord Basin.

Numerical forward modelling has shown that variations in lithospheric and asthenospheric rheology, varying crustal strength profiles during rifting, length of interrift period(s), and overall extension velocity are factors controlling rift axis migration and rift basin abandonment (Tett & Sawyer; Braun, 1992; Bertotti *et al.*, 1997; van Wijk & Cloetingh, 2002; Huismans & Beaumont, 2011; Brune *et al.*, 2014; Naliboff & Buiter, 2015; Svartman Dias *et al.*, 2015; Tetreault & Buiter, 2018). Assuming the Late Permian-Early Triassic rift phase lasted for ca. 20 million years (Steel & Ryseth, 1990) and was associated with a stretching factor of β=1.55 ±10% in the Stord Basin (this study), this would correspond to an extension velocity of ca. 2 mm/yr; this is considered as ultraslow (Pérez-Gussinyé & Reston, 2001; Welford *et al.*, 2010; Tetreault & Buiter, 2018). Numerical modelling by Tetreault & Buiter, 2018 shows that ultraslow extension result in increased crust-mantle coupling and the creation of symmetric margins. Although crustal extension in the Stord Basin stops long before continental

488 breakup, the basin is symmetric (Fig. 2C). Such a slow extension rate might therefore explain the
489 symmetry of the Stord Basin. Numerical models suggest that the rift abandonment will occur either
490 by ultraslow extension rate or by a long period of tectonic quiescence between extension episodes
491 (van Wijk & Cloetingh, 2002; Naliboff & Buiter, 2015). Here in the Stord Basin we have a combination
492 of ultraslow extension (ca. 2 mm/yr), which possibly lead to magmatic underplating, changes in the
493 crustal strength profile, and a long period of tectonic quiescence (~70 myr) between RP1 and RP2.
494 These factors together may have caused lithospheric hardening, rift basin abandonment and rift axis
495 migration, despite a relatively high amount of extension (β=1.55 ±10%) in the Stord Basin during RP1.
496 Similarly, rift basins that developed during the Permo-Triassic, Late Jurassic-Early Cretaceous, and Late
497 Cretaceous-Early Tertiary along the mid-Norwegian margin were abandoned as strain migrated overall
498 westward-to-northwestward, away from the Norwegian mainland (Gabrielsen *et al.*, 1999; Reemst &
499 Cloetingh, 2000).

500 ***Influence of preexisting structures on rift fault strike and activity***

501 The Øygarden Fault System (ØFS) bounds the Stord Basin to the east and consists of four main
502 segments in the study area (Fig. 1 and 2A). The west-dipping ØFS3 segment strikes N-S over a 30 km
503 extent from its northern tip, which then gradually rotates to an NNE-SSW orientation. This strike
504 rotation of ca. 25° occurs close (N59°.33') to the southwestern tip of an onshore section of the
505 Hardangerfjord Shear Zone (HSZ, Fig. 1 and 2A). Farther south, ØFS3 strikes subparallel to the offshore
506 extension of the HSZ (Fig. 2A, Fazlikhani *et al.*, 2017). The southern segments, ØFS4 and ØFS5, show
507 an abrupt change in strike of ca. 50° for ØFS4 and 45° for ØFS5 near the offshore extension of the HSZ
508 (Fig. 2A). This shear zone, therefore, appears to play a clear role in the development of the ØFS
509 structural style.

510 Along the western margin of the Stord Basin, the Utsira East Fault (UEF) is aligned with the Utsira Shear
511 Zone (USZ, Figs. 1 and 2A). UEF1 strikes NE-SW, parallel to the NE-SW-striking portion of the USZ, and
512 both trend oblique to the regional E-W extension direction for RP1. However, UEF2 is not aligned with
513 the USZ trend and instead strikes almost N-S, perpendicular to the regional E-W extension direction
514 (Fig. 2A). At this location, both the regional stress field related to the E-W extension direction, and the
515 local stress field near the pre-existing USZ, played key roles in controlling rift fault geometry and the
516 development of two fault trends. Further south, UEF3 and UEF4 are aligned with, and most likely,
517 reactivated the USZ. Also here, the variable influence of the pre-existing USZ on the regional E-W
518 extension caused the development of rift faults of variable orientation. In the southwestern edge of
519 the basin, UEF5 strikes NW-SE; it is not therefore aligned with the USZ nor perpendicular to the
520 regional stress field. Here other factors, such as lithological differences between the Utsira High

(strong basement) and southern parts of the Stord Basin, may have promoted strain localization and controlled the geometry of UEF5 (Bott, M.H.P., Day, A.A., Masson-Smith, D., 1958; Castro *et al.*, 2007; Howell *et al.*, 2019; Phillips *et al.*, 2019) .

North of the Stord Basin (at 60° N, Fig. 1), the USZ strikes NEE-SWW, sub-parallel to the regional E-W extension direction (Fig. 2A). Rift fault F1 strikes overall N-S (Fig. 1), although with tips of individual fault segments have a more NE-SW strike. F1 develops perpendicular to the E-W regional extension direction and offsets the USZ. However, rotated segment tips are subparallel to the USZ, most likely associated with mylonitic foliation or layering within the shear zone, both of which may be prone to being preferentially reactivated (Paton & Underhill, 2004; Gontijo-Pascutti *et al.*, 2010; Kirkpatrick *et al.*, 2013; Salomon *et al.*, 2015; Morley, 2017; Heilman *et al.*, 2019). In this case, the orientation of the regional stress field is the primary factor controlling rift fault development, whilst the presence of pre-existing structures influences segment tip reorientation.

Within the basin, rift faults (F2, F3 and some minor faults) mainly strike N-S (Fig. 2A) and developed perpendicular to the regional E-W extension direction. The exception is F4, which strikes NE-SW, as well as some segments of F1 and F2 (Fig. 2A). This may be due to rotation of the local stress by pre-rift basement structures parallel to the HSZ trend that are not imaged in the available seismic data.

A logarithmic fault displacement-length plot of the studied RP1 faults (Fig. 11) shows that all studied rift faults and fault segments plot between D=L/10 and D=L/100 lines, whereas RP2 fault segments cluster around D=L/100 and towards D=L/1000 lines. Comparing our obsrvation with the global displacement vs. length compilation (Schultz *et al.*, 2008 and references therin) suggests that RP2 faults are under-displaced relative to their length (Fig. 11). Although observed low displacement-length may not necessarily be caused by structural inheritance (see Rotevatn *et al.*, 2019), since the study area is located within a very heterogenous crust experiencing several deformation phases, we suggest that the observed low displacement-length ratio here may be related to the influence of structural inheritance. Faults in the Stord Basin strike N-S, NE-SW and NW-SE (e.g. compare faults on time-structure map in Fig. 2A), similar to the trend of pre-existing structures related to the Caledonian and/or post-orogenic Devonian tectonic events. These structures may have locally perturbed the regional stress field and influenced rift fault strike and kinematics in the early stages of fault development (cf. Collanega *et al.*, 2019; Osagiede *et al.*, 2019). Later, as extension continues, and fault segments grew and linked laterally, rift fault activity focuses on fault segments that strike at a high-angle (e.g. N-S) to the E-W regional stress field.

Permo-Triassic (RP1) and Middle Jurassic-Lower Cretaceous (RP2) rifting in the Stord Basin and northern North Sea

Activity of RP1 faults in the Stord Basin created significant accommodation for syn-rift sediments to accumulate (Fig. 4A and 4B). The thickest early syn-RP1 depocentres are distributed across the basin, (Fig. 4A), which contrasts with the late syn-RP1 phase depocentres that localize occur next to the basin-bounding UEF and ØFS faults (Fig. 4B). The earliest stages of RP1 are therefore characterized by distributed faulting and associated depocentres. However, as faults continue to grow, the basin-bounding faults develop as the key strain-accommodating structures, storing the thickest sediments in the hanging wall. During early post-RP1, almost the entire Stord Basin accumulates more than 400 ms (ca. 300 m) of sediments (Fig. 6A). During this phase, all the basin centre rift faults are buried, and depocentres only develop adjacent to basin-bounding ØFS and UEF faults. During the late post-RP1, thickness of sediments is >400 ms, except in the hanging wall of UEF2 and 3 (Fig. 6B). This highlights that by the late post-RP1 almost all accommodation created during RP1 was filled (Fig. 6B). It appears that select N-S-striking faults preferentially accrue strain during the early post-RP1 stage and therefore focus deposition in these locations. We would expect these fault segments to preferentially slip under an E-W oriented minimum stress direction, particularly if the extension rate has decreased during the post-rift subsidence phase.

During the Middle Jurassic to Late Cretaceous, the Stord Basin is characterized by relatively little tectonic activity, and sedimentary loading is a key process in creating sediment accommodation. The westward-prograding Hardangerfjord Delta, is a significant depositional feature. The Hardangerfjord Delta is most likely developed during Upper Jurassic (Jarsve *et al.*, 2014) and is not affected by Late Jurassic rift faults. The Hardangerfjord Delta does not extend north of 60°N and is separated from the Brent Delta by the Brage Horst and Oseberg Fault Block, near the Lomre Shear Zone (Deng *et al.*, 2017a; Fazlikhani *et al.*, 2017). Lower Cretaceous deep-marine sediments (Cromer Knoll Group) preferentially fill accommodation north and south of the Hardangerfjord Delta (Fig. 7B).

Basin-bounding rift faults in the Stord Basin are active throughout the RP1 syn- and post-rift periods and into RP2, during which times they accrued only up to 250-300 m of throw. By contrast, in the northern Horda Platform, RP1 faults are reactivated during early post-RP2 and developed throws of up to 650-700 m (Bell *et al.*, 2014; Whipp *et al.*, 2014; Duffy *et al.*, 2015; Deng *et al.*, 2017a). Such diachronous fault activity during RP2 suggests an overall northward migration of strain offshore Norway between rift phases. This is in consistent with the slightly higher RP2 β values calculated in the northern Horda Platform compared to the southern Horda Platform (i.e. Stord Basin, Table 1). Farther north, between 61° and 62°N, the Måløy Slope area was only extended during RP2, whereas

586 basins further west, such as the northern Viking Graben and East Shetland Basin, were extended
587 during both rifting phases (Lenhart *et al.*, 2019; Phillips *et al.*, 2019). On the eastern side of the Viking
588 Graben, three distinct areas are identified: 1) 59°-60°N, where highly extended areas during RP1 (i.e.
589 Stord Basin) are almost abandoned during RP2, 2) 60°-61°N, where rift faults in the moderately-
590 extended northern Horda Platform reactivate during RP2, and 3) 61°-62°N, where the Måløy slope is
591 mainly extended during RP2.

592 Within the Stord Basin, fault activity during RP2 was mainly localized along the basin-bounding UEF
593 and ØFS faults. Here, long-lived, easterly dipping UEF fault segments, which dip away from the new
594 RP2 rift axis in the Viking Graben, accommodated Late Jurassic extension. This contrasts with the East
595 Shetland Basin, which defines the opposite side of the RP2 rift-axis, where newly initiated, easterly-
596 dipping faults (i.e. towards the rift axis) cross-cut pre-existing, westerly-dipping, RP1 structures
597 (Tomasso *et al.*, 2008; Claringbould *et al.*, 2017). Comparing the timing of faulting in the Stord Basin
598 (i.e. southern Horda Platform), northern Horda Platform, and East Shetland Basin shows that: a) RP1
599 faults in the Stord Basin are continuously active during syn- and post-RP1, and during syn-RP2. Instead
600 of new rift faults initiating during RP2, the easterly-dipping UEF fault accommodates the majority of
601 RP2 rift-related strain; b) in the northern Horda Platform, RP1 faults reactivate in late syn-RP2 and
602 early post-RP2 (Bell *et al.*, 2014; Whipp *et al.*, 2014; Duffy *et al.*, 2015; Deng *et al.*, 2017a; Phillips *et*
603 *al.*, 2019); and c) RP1 faults in the East Shetland Basin are cross-cut by easterly dipping RP2 faults
604 (Tomasso *et al.*, 2008; Claringbould *et al.*, 2017). Our study, in addition to data from other areas of the
605 northern North Sea, provide an example of the patterns of strain migration, and fault initiation and
606 reactivation, that can occur during multiphase continental extension. The rift kinematics documented
607 here may be more broadly applicable to areas formed in response to multiphase extension of strongly
608 heterogenous crust.

609

610

611 **Conclusions**

612 Seismo-stratigraphic and structural evolution of the Stord Basin, offshore southern Norway
613 documents the development of a rift basin in two rift phases. Our key findings can be summarized as
614 follows:

615

616 • The Stord Basin, located in the southern Horda Platform, developed during the Permo-Triassic
617 rifting phase (RP1) with a stretching factor up to β=1.55 (±10%). The Stord Basin was

abandoned during the Late Jurassic-Early Cretaceous rift phase (RP2, β=1.01 ± 10%) despite being the most extended area in the northern North Sea rift during RP1. This may be due to the ultraslow extension (<2mm/yr) and the long period of tectonic quiescence (ca. 70 myr) between RP1 and RP2 leading to changes in lithospheric strength profile and possible underplating, which in turn lead to the westward rift relocation to the Viking Graben during RP2.

- The earliest stages of RP1 are characterized by distributed faulting with associated depocentres, however as faults continue to develop the basin-bounding faults become the key strain-accommodating structures with associated sediment depocentres. Between syn- and post-RP1 strain migrates to the west from the Øygarden Fault System to the Utsira East Fault and migrates southward along the basin.

- The kilometre-scale basin geometry is controlled by a) E-W extension, and b) the presence of pre-existing Caledonian/Devonian structures, namely the Utsira Shear Zone (USZ) in the west and Hardangerfjord Shear Zone (HSZ) in the east. Smaller-scale pre-rift basement structures might account for fault segment tip reorientation during RP1.

- RP2 fault throw decreases to ca. 10-20% of that accumulated during RP1, although active fault length is ca. 75-80% of active fault length during RP1. During RP2, strain migrates overall northwards into the northern Horda Platform. Sedimentation patterns are primarily controlled by basin thermal subsidence during RP2, and key depocentres are associated with, or adjacent to, the Middle to Late Jurassic Hardangerfjord Delta.

- RP1 faults across the northern North Sea react differently to RP2 extension: in a) the Stord Basin RP1 faults are continuously active during syn- and post-RP1 and into syn-RP2. Rift faults in the centre of the basin are only active up to Early post-RP1, b) northern Horda Platform RP1 faults reactivate during Late syn-RP2 and Early post-RP2, and c) in the East Shetland Basin, RP1 faults are mainly cross-cut by RP2 faults.

Our study documents a rift basin abandonment and rift axis migration in northern North Sea multirifted basin. We have shown that rift fault activtity migrates during and after rift climax and controls main rift depocenters. This result reflects the general complexity of rift basin evolution in multirfited regions.

Acknowledgment

This contribution forms part of the MultiRift Project funded by the Research Council of Norway (PETROMAKS project 215591/E30) and Equinor to the University of Bergen and partners Imperial College, University of Manchester, and University of Oslo. Hamed Fazlikhani is funded by the Geothermal Allinz Bavaria (GAB) at the Friedrich Alexander Universität Erlangen - Nürnberg. The seismic data used in this study are publicly available for download via the DISKOS online portal (https://portal.diskos.cgg.com). Thanks to TGS and Bent Erlend Kjølhamar for permission to publish the seismic data and to Schlumberger for providing academic licenses for the use of Petrel at the University of Bergen and Friedrich Alexander Universität Erlangen - Nürnberg. We would also like to thank the VISTA program for supporting the professorship of Rob Gawthorpe. All members of the MultiRift project are thanked for the fruitful discussions throughout the project.

Figure Caption

Figure 1: Location of the Stord Basin in the northern North Sea, offshore southern Norway shown by blue dashed line. Time-structure map of Base Rift (Base RP1) shows general structural configuration in the northern North Sea. Thin black lines in the background show 2D seismic profiles utilized in this study. Red dotes are exploration wells used for well-seismic tie and stratigraphic correlation.

Figure 2: A) Base RP1 time-structure map of the Stord Basin and neighbouring Utsira High to the west and Stavanger Platform to the east. Main basin bounding faults are Øygarden Fault System (ØFS) and Utsira East Fault (UEF), each consisting of several segments. Location of underlying Caledonian/Devonian Utsira Shear Zone (USZ), Hardangerfjord Shear Zone (HSZ) and Øygarden Shear Zone (ØSZ) are shown, projected to the Base RP1 surface (transparent white polygons). Wells used in seismic well-tie are shown in red (basement drilled) and black. B) Simplified stratigraphic chart and main interpreted horizons in the Stord Basin. C) Regional seismic profile (NSR-41153, courtesy of TGS) across the Stord Basin, Utsira High, south Viking Graben and East Shetland Platform. Three main tectono-stratigraphic units are Permo-Triassic (RP1) syn and postrift, Middle Jurassic - Early Cretaceous (RP2) syn and postrift covered by Cenozoic to present day postrift units.

Figure 3: Interpreted seismic cross sections showing seven key horizons above Base RP1 surface. See Fig. 2A for locations. A (NSR-11152, courtesy of TGS) and B (NSR06-22356, courtesy of TGS) show the western margin of the Stord Basin and the Utsira East Fault (UEF). C (SBGS-R94-002, courtesy of TGS)

684 and D (GNSR-91-149, courtesy of Norwegian Petroleum Directorate) show eastern margin of the Stord
685 basin and the Øygarden Fault System (ØFS).

686 **Figure 4:** Time-thickness maps of A) early syn-RP1 and B) late syn-RP1. Highlighted faults show the
687 length of the fault that is active during syn-RP1.

688 **Figure 5:** Active fault length (km) vs. tectonic event plots showing changes in fault length during syn
689 and postrift events measured on time-thickness maps. Percentages marked on the graphs show the
690 amount of fault expansion or shortening. A) Active fault length along ØFS segments, B) Active length
691 of UEF segments and C) Active fault length plot for the rift faults located in the centre of the Stord
692 Basin. Note that only for ØFS3 and F3 does the active fault length increase significantly during the syn-
693 RP2. Here F3 is reactivated along almost 50% of its initial length and ØFS3 active length increase by
694 220% in compare to Late post-RP1.

695 **Figure 6:** Time-thickness maps of A) early post-RP1 and B) late post-RP1. Active fault length is shown
696 as white lines. The main early post-RP1 depocentre is located in the hanging wall of ØFS3 and F1 and
697 migrates westward to the hanging wall of UEF2 and UEF3 during late post-RP1 time.

698 **Figure 7:** Time-thickness maps of RP2. A) syn-RP2, showing main depocentre and active faults during
699 Middle and Upper Jurassic. B) lower Cretaceous post-RP2. C) upper Cretaceous post-RP2. Thickness
700 maximum in the centre of the Stord Basin during syn-RP2 is related to westward propagating
701 Hardangerfjord Delta (see Fig. 8). Late Cretaceous post-RP2 is marked by a general thin and evenly
702 distributed package of sediments in the Stord Basin.

703 **Figure 8:** A) Uninterpreted and B) interpreted section across the eastern Stord Basin showing syn- and
704 post-RP1 and RP2 studied units (courtesy of TGS). RP1 ØFS3 and F3 faults offset Middle Jurassic surface
705 by 110 ms and 130 ms of throw respectively. C) Development of the Hardangerfjord Delta in the Stord
706 Basin synchronous with syn-RP2 fault activities in the northern Horda Platform, Viking Graben and
707 East Shetland Basin.

708 **Figure 9:** Time structure map of Base rift surface in the centre. Along-strike throw values are
709 backstripped and depth converted based on the velocity-depth relationship from checkshot data.
710 Upper and lower curves represent error margins related to the depth conversion. Throw values on the
711 Base RP1 surface show fault activity during RP1, and throw values at Base Middle Jurassic (Base Brent
712 Group) level show fault activity during RP2. Fault throw vs. fault length graphs highlights lateral fault
713 throw distribution during RP1 and RP2 in the Stord Basin.

714 **Figure 10:** Compilation of calculated amount of extension (β-factor) for RP1 (red values) and RP2 (blue
715 values) in the northern North Sea Basin. β values in the Stord basin are calculated using the fault heave

716 summation method (see text for discussion). Values along the long dashed line (deep seismic section
717 NSDP-1) are calculated using forward modelling with initial crustal thickness T_o=35 km (Odinsen *et al.*,
718 2000b). Dotted lines show cross sections from (Roberts *et al.*, 1995) where β values were calculated
719 using backstripping and reversed modelling (note that the RP2 β values are measured close to the
720 dotted sections of Roberts *et al.*, 1993. Port-rift (T_1) crustal thickness T_1= 16, T_1= 21 and T_1= 26 contour
721 lines (continuous black lines) are from Klemperer, 1988 that are used to calculate β values (for total
722 amount of extension that is not differentiated between rifting phases) in northern North Sea basin.
723 Stars show the values calculate using fault throws by (Bell *et al.*, 2014) in the northern Horda Platform
724 (not corrected for sudseismic faulting). Thick black lines are β values estimated in this study.

725 **Figure 11:** Global compilation of fault displacement versus fault length plot (Dmax/L, from Schultz *et*
726 *al.*, 2008) overlaid by RP1 and RP2 fault displacement and length measurements. Enlarged graph
727 shows fault displacement and length for Øygarden Fault System segments (green circles), Utsira East
728 Fault segments (violet circles) and intra-basin faults (yellow circles) in detail. RP2 faults are under-
729 displaced relative to the fault length, suggesting the reactivation of RP1 faults during RP2.

730 **Table 1:** Amount of extension (β-factor) measured across the northern and southern Stord Basin
731 during the RP1 and RP2. In order to account for contribution of subseismic faults 30% is added to the
732 measured values. See text for details.

733 **Appendix 1:** Illustration of methods used to measure fault vertical displacement (throw). A) Seismic
734 section (NSR-42357, courtesy of TGS) across the UEF3. B) Geo-seismic section showing an example of
735 throw summation across a vertically multisegmented rift fault. C) Shows Base RP1 time-structure map,
736 rift faults and created synthetic sections. D) 2D seismic profiles and synthetic sections created
737 perpendicular to fault strike. Interpreted horizons based on 2D seismic profiles are projected into
738 these synthetic sections, allowing fault throw and heave measurements perpendicular to fault strike.
739 E) An example of synthetic section where projection of interpreted horizons are shown. Red squares
740 show footwall cutoff and blue squares are hanging wall cutoff in D and E.

741 **Appendix 2:** Time-structure maps of interpreted horizons in the Stord Basin. These surfaces are used
742 to create time-thickness maps. White lines are rift faults displacing time-structure maps.

743

744

745 References

BADLEY, M.E., EGEBERG, T. & NIPEN, O. (1984) Development of rift basins illustrated by the structural evolution of the Oseberg feature, Block 30/6, offshore Norway. *Journal of the Geological Society*, **141** (4), 639. doi:10.1144/gsjgs.141.4.0639

BADLEY, M.E., PRICE, J.D., RAMBECH DAHL, C. & AGDESTEIN, T. (1988) The structural evolution of the northern Viking Graben and its bearing upon extensional modes of basin formation. *Journal of the Geological Society*, **145** (3), 455–472. doi:10.1144/gsjgs.145.3.0455

BELL, R.E., JACKSON, C.A.-L., WHIPP, P.S. & CLEMENTS, B. (2014) Strain migration during multiphase extension: Observations from the northern North Sea. *Tectonics*, **33** (10), 1936–1963. doi:10.1002/2014TC003551

BERTOTTI, G., TER VOORDE, M., CLOETINGH, S. & PICOTTI, V. (1997) Thermomechanical evolution of the South Alpine rifted margin (North Italy): constraints on the strength of passive continental margins. *Earth and Planetary Science Letters*, **146** (1), 181–193. doi:10.1016/S0012-821X(96)00214-2

BOTT, M.H.P., DAY, A.A., MASSON-SMITH, D. (1958) The geological interpretation of gravity and magnetic surveys in Devon and Cornwall. *Philosophical Transactions of the Royal Society of London. Series A: Mathematical, Physical and Engineering Sciences*, **251** (992), 161–191. doi:10.1098/rsta.1958.0013

BRANSDEN, P.J.E., BURGES, P., DURHAM, M.J. & HALL, J.G. (1999) Evidence for multi-phase rifting in the North Falklands Basin. *Geological Society, London, Special Publications*, **153** (1), 425. doi:10.1144/GSL.SP.1999.153.01.26

BRAUN, J. (1992) Postextensional mantle healing and episodic extension in the Canning Basin. *J. Geophys. Res.*, **97** (B6), 8927–8936. doi:10.1029/92JB00584

BRUNE, S., HEINE, C., PÉREZ-GUSSINYÉ, M. & SOBOLEV, S.V. (2014) Rift migration explains continental margin asymmetry and crustal hyper-extension. *Nature communications*, **5** (1), 4014. doi:10.1038/ncomms5014

CASTRO, D.L. de, OLIVEIRA, D.C. de & GOMES CASTELO BRANCO, RAIMUNDO MARIANO (2007) On the tectonics of the Neocomian Rio do Peixe Rift Basin, NE Brazil: Lessons from gravity, magnetics, and radiometric data. *Journal of South American Earth Sciences*, **24** (2), 184–202. doi:10.1016/j.jsames.2007.04.001

CHILDS, C., NICOL, A., WALSH, J.J. & WATTERSON, J. (2003) The growth and propagation of synsedimentary faults. *Geol*, **25** (4), 633–648. doi:10.1016/S0191-8141(02)00054-8

CLARINGBOULD, J.S., BELL, R.E., JACKSON, C.A.-L., GAWTHORPE, R.L. & ODINSEN, T. (2017) Pre-existing normal faults have limited control on the rift geometry of the northern North Sea. *Earth and Planetary Science Letters*, **475**, 190–206. doi:10.1016/j.epsl.2017.07.014

COLLANEGA, L., SIUDA, K., A.-L. JACKSON, C., BELL, R.E., COLEMAN, A.J., LENHART, A., MAGEE, C. & BREDA, A. (2019) Normal fault growth influenced by basement fabrics: The importance of preferential nucleation from pre-existing structures. *Basin Res*, **31** (4), 659–687. doi:10.1111/bre.12327

DENG, C., FOSSEN, H., GAWTHORPE, R.L., ROTEVATN, A., JACKSON, C.A.-L. & FAZLIKHANI, H. (2017a) Influence of fault reactivation during multiphase rifting: The Oseberg area, northern North Sea rift. *Marine and Petroleum Geology*, **86**, 1252–1272. doi:10.1016/j.marpetgeo.2017.07.025

DENG, C., GAWTHORPE, R.L., FINCH, E. & FOSSEN, H. (2017b) Influence of a pre-existing basement weakness on normal fault growth during oblique extension: Insights from discrete element modeling. *Geol*, **105**, 44–61. doi:10.1016/j.jsg.2017.11.005

DUFFY, O.B., BELL, R.E., JACKSON, C.A.-L., GAWTHORPE, R.L. & WHIPP, P.S. (2015) Fault growth and interactions in a multiphase rift fault network: Horda Platform, Norwegian North Sea. *Journal of Structural Geology*, **80**, 99–119. doi:10.1016/j.jsg.2015.08.015

FÆRSETH, R.B. (1996) Interaction of Permo-Triassic and Jurassic extensional fault-blocks during the development of the northern North Sea. *Journal of the Geological Society*, **153** (6), 931. doi:10.1144/gsjgs.153.6.0931

FÆRSETH, R.B., GABRIELSEN, R. H. & HURICH, C.A. (1995) Influence of basement in structuring of the North Sea basin, offshore southwest Norway. *Norwegian Journal of Geology*, **75**, 105–119.

FAZLIKHANI, H. & BACK, S. (2015) The influence of differential sedimentary loading and compaction on the development of a deltaic rollover. *Marine and Petroleum Geology*, **59**, 136–149. doi:10.1016/j.marpetgeo.2014.08.005

FAZLIKHANI, H., FOSSEN, H., GAWTHORPE, R.L., FALEIDE, J.I. & BELL, R.E. (2017) Basement structure and its influence on the structural configuration of the northern North Sea rift. *Tectonics*, **36** (6), 1151–1177. doi:10.1002/2017TC004514

FOSSEN, H. (1992) The role of extensional tectonics in the Caledonides of south Norway. *Geol*, **14** (8), 1033–1046. doi:10.1016/0191-8141(92)90034-T

FOSSEN, H. & DUNLAP, W.J. (1999) On the age and tectonic significance of Permo-Triassic dikes in the Bergen-Sunnhordland region, southwestern Norway. *Norsk Geologisk Tidsskrift*, **79** (3), 169–178. doi:10.1080/002919699433807

FOSSEN, H., FAZLIKHANI, H., FALEIDE, J.I., KSIENZYK, A.K. & DUNLAP, W.J. (2016) Post-Caledonian extension in the West Norway–northern North Sea region: the role of structural inheritance. *Geological Society, London, Special Publications*, **439** (1), 465. doi:10.1144/SP439.6

FOSSEN, H. & HURICH, C.A. (2005) The Hardangerfjord Shear Zone in SW Norway and the North Sea: a large-scale low-angle shear zone in the Caledonian crust. *Journal of the Geological Society*, **162** (4), 675. doi:10.1144/0016-764904-136

FOUCHER, J.-P., LE PICHON, X. & SIBUET, J.C. (1982) The ocean-continent transition in the uniform lithospheric stretching model: role of partial melting in the mantle.

GABRIELSEN, R.H., ODINSEN, T. & GRUNNALEITE, I. (1999) Structuring of the Northern Viking Graben and the Møre Basin; the influence of basement structural grain, and the particular role of the Møre-Trøndelag Fault Complex. *Marine and Petroleum Geology*, **16** (5), 443–465. doi:10.1016/S0264-8172(99)00006-9

GABRIELSEN, R. H., FÆRSETH, R.B., STEEL, R.J. & IDIL, S. AND KLØVJAN, O. S. (1990) Architectural styles of basin fill in the northern Viking Graben. *Tectonic evolution of the North Sea rifts*, 158–179.

GABRIELSEN, R. H., KYRKJEBØ, R., FALEIDE, J.I., FJELDSKAAR, W. & AND KJENNERUD, T. (2001) The Cretaceous post-rift basin configuration of the northern North Sea.

GONTIJO-PASCUTTI, A., BEZERRA, F.H.R., LA TERRA, E. & ALMEIDA, J.C.H. (2010) Brittle reactivation of mylonitic fabric and the origin of the Cenozoic Rio Santana Graben, southeastern Brazil. *Journal of South American Earth Sciences*, **29** (2), 522–536. doi:10.1016/j.jsames.2009.06.007

HEEREMANS, M. & FALEIDE, J.I. (2004) Late Carboniferous-Permian tectonics and magmatic activity in the Skagerrak, Kattegat and the North Sea. *Geological Society, London, Special Publications*, **223** (1), 157. doi:10.1144/GSL.SP.2004.223.01.07

HEILMAN, E., KOLAWOLE, F., ATEKWANA, E.A. & MAYLE, M. (2019) Controls of Basement Fabric on the Linkage of Rift Segments. *Tectonics*, **38** (4), 1337–1366. doi:10.1029/2018TC005362

HOWELL, L., EGAN, S., LESLIE, G. & CLARKE, S. (2019) Structural and geodynamic modelling of the influence of granite bodies during lithospheric extension: Application to the Carboniferous basins of northern England. *Tectonophysics*, **755**, 47–63. doi:10.1016/j.tecto.2019.02.008

HUISMANS, R. & BEAUMONT, C. (2011) Depth-dependent extension, two-stage breakup and cratonic underplating at rifted margins. *Nature*, **473** (7345), 74–78. doi:10.1038/nature09988

JACKSON, C.A.-L. & LEWIS, M.M. (2013) Physiography of the NE margin of the Permian Salt Basin: new insights from 3D seismic reflection data. *Journal of the Geological Society*, **170** (6), 857. doi:10.1144/jgs2013-026

JACKSON, C.A.-L. & ROTEVATN, A. (2013) 3D seismic analysis of the structure and evolution of a salt-influenced normal fault zone: A test of competing fault growth models. *Geol*, **54**, 215–234. doi:10.1016/j.jsg.2013.06.012

JARSVE, E.M., FALEIDE, J.I.N., GABRIELSEN, R.H.Y. & NYSTUEN, J.P. (2014a) *Mesozoic and cenozoic basin configurations in the North Sea*.

JARSVE, E.M., MAAST, T.E., GABRIELSEN, R.H., FALEIDE, J.I., NYSTUEN, J.P. & SASSIER, C. (2014b) Seismic stratigraphic subdivision of the Triassic succession in the Central North Sea; integrating seismic

reflection and well data. *Journal of the Geological Society*, **171** (3), 353–374. doi:10.1144/jgs2013-056

KIERSNOWSKI, H., PAUL, J., PERYT, T.M. & AND SMITH, D.B. (1995) Facies, Paleogeography, and Sedimentary History of the Southern Permian Basin in Europe.

KIM, Y.-S. & SANDERSON, D.J. (2005) The relationship between displacement and length of faults: a review. *Earth-Science Reviews*, **68** (3), 317–334. doi:10.1016/j.earscirev.2004.06.003

KIRKPATRICK, J.D., BEZERRA, F.H.R., SHIPTON, Z.K., DO NASCIMENTO, A.F., PYTHAROULI, S.I., LUNN, R.J. & SODEN, A.M. (2013) Scale-dependent influence of pre-existing basement shear zones on rift faulting: a case study from NE Brazil. *Journal of the Geological Society*, **170** (2), 237. doi:10.1144/jgs2012-043

KLEMPERER, S.L. (1988) Crustal thinning and nature of extension in the northern North Sea from deep seismic reflection profiling. *Tectonics*, **7** (4), 803–821. doi:10.1029/TC007i004p00803

KSIENSYK, A.K., WEMMER, K., JACOBS, J., FOSSEN, H., SCHOMBERG, A.C., SÜSSENBERGER, A.N., LÜNSDORF, K. & BASTESEN, E. (2016) Post-Caledonian brittle deformation in the Bergen area, West Norway: results from K–Ar illite fault gouge dating. *NJG*, **96** (3), 275–299.

LENHART, A., JACKSON, C.A.-L., BELL, R.E., DUFFY, O.B., GAWTHORPE, R.L. & FOSSEN, H. (2019) Structural architecture and composition of crystalline basement offshore west Norway. *Lithosphere*, **11** (2), 273–293. doi:10.1130/L668.1

LERVIK, K.S. (2006) Triassic lithostratigraphy of the northern North Sea Basin. *Norwegian Journal of Geology*, **86**, 93–116.

LONG, J.J. & IMBER, J. (2010) Geometrically coherent continuous deformation in the volume surrounding a seismically imaged normal fault-array. *Geol*, **32** (2), 222–234. doi:10.1016/j.jsg.2009.11.009

LUNDIN, E.R. & DORÉ, A.G. (1997) A tectonic model for the Norwegian passive margin with implications for the NE Atlantic: Early Cretaceous to break-up. *Journal of the Geological Society*, **154** (3), 545. doi:10.1144/gsjgs.154.3.0545

MARRETT, R. & ALLMENDINGER, R.W. (1992) Amount of extension on "small" faults: An example from the Viking graben. *Geol*, **20** (1), 47. doi:10.1130/0091-7613(1992)020<0047:AOEOSF>2.3.CO;2

MCKENZIE, D. (1978) Some remarks on the development of sedimentary basins. *Earth and Planetary Science Letters*, **40** (1), 25–32. doi:10.1016/0012-821X(78)90071-7

MCKENZIE, D.A.N. & O'NIONS, R.K. (1991) Partial Melt Distributions from Inversion of Rare Earth Element Concentrations. *petrology*, **32** (5), 1021–1091. doi:10.1093/petrology/32.5.1021

MCLEOD, A.E., DAWERS*, N.H. & UNDERHILL, J.R. (2000) The propagation and linkage of normal faults: insights from the Strathspey–Brent–Statfjord fault array, northern North Sea. *Basin Res*, **12** (3-4), 263–284. doi:10.1111/j.1365-2117.2000.00124.x

MORLEY, C.K. (1996) Discussion of potential errors in fault heave methods for extension estimates in rifts, with particular reference to fractal fault populations and inherited fabrics. *Geological Society, London, Special Publications*, **99** (1), 117. doi:10.1144/GSL.SP.1996.099.01.10

MORLEY, C.K. (2017) The impact of multiple extension events, stress rotation and inherited fabrics on normal fault geometries and evolution in the Cenozoic rift basins of Thailand. *Geological Society, London, Special Publications*, **439** (1), 413. doi:10.1144/SP439.3

NALIBOFF, J. & BUITER, S.J.H. (2015) Rift reactivation and migration during multiphase extension. *Earth and Planetary Science Letters*, **421**, 58–67. doi:10.1016/j.epsl.2015.03.050

ODINSEN, T., CHRISTIANSSON, P., GABRIELSEN, ROY, H & FALEIDE, JAN, INGE & BERGE, ANKER, M. (2000a) The geometries and deep structure of the northern North Sea rift system.

ODINSEN, T., REEMST, P., VAN DER BEEK, P., FALEIDE, J.I. & GABRIELSEN, R.H. (2000b) Permo-Triassic and Jurassic extension in the northern North Sea: results from tectonostratigraphic forward modelling. *Geological Society, London, Special Publications*, **167** (1), 83–103. doi:10.1144/GSL.SP.2000.167.01.05

OSAGIEDE, E.E., ROTEVATN, A., GAWTHORPE, R., KRISTENSEN, T.B., JACKSON, C.A.-L. & MARSH, N. (2019) Pre-existing intra-basement shear zones influence growth and geometry of non-colinear normal

faults, western Utsira High–Heimdal Terrace, North Sea. *Geol*, 103908. doi:10.1016/j.jsg.2019.103908

OSMUNDSEN, P.T. & ANDERSEN, T.B. (1994) Caledonian compressional and late-orogenic extensional deformation in the Staveneset area, Sunnfjord, Western Norway. *Geol*, **16** (10), 1385–1401. doi:10.1016/0191-8141(94)90004-3

PATON, D.A. (2006) Influence of crustal heterogeneity on normal fault dimensions and evolution: southern South Africa extensional system. *Journal of Structural Geology*, **28** (5), 868–886. doi:10.1016/j.jsg.2006.01.006

PATON, D.A. & UNDERHILL, J.R. (2004) Role of crustal anisotropy in modifying the structural and sedimentological evolution of extensional basins: the Gamtoos Basin, South Africa. *Basin Res*, **16** (3), 339–359. doi:10.1111/j.1365-2117.2004.00237.x

PEACOCK, D.C.P. & SANDERSON, D.J. (1991) Displacements, segment linkage and relay ramps in normal fault zones. *Geol*, **13** (6), 721–733. doi:10.1016/0191-8141(91)90033-F

PÉREZ-GUSSINYÉ, M. & RESTON, T.J. (2001) Rheological evolution during extension at nonvolcanic rifted margins: Onset of serpentinization and development of detachments leading to continental breakup. *J. Geophys. Res.*, **106** (B3), 3961–3975. doi:10.1029/2000JB900325

PETERSEN, K., CLAUSEN, O.R. & KORSTGÅRD, J.A. (1992) Evolution of a salt-related listric growth fault near the d-1 well, block 5605, danish north sea: displacement history and salt kinematics. *Geol*, **14** (5), 565–577. doi:10.1016/0191-8141(92)90157-R

PHILLIPS, T.B., FAZLIKHANI, H., GAWTHORPE, R.L., FOSSEN, H., JACKSON, C.A.-L., BELL, R.E., FALEIDE, J.I. & ROTEVATN, A. (2019) The Influence of Structural Inheritance and Multiphase Extension on Rift Development, the NorthernNorth Sea. *Tectonics*, **n/a** (n/a). doi:10.1029/2019TC005756

PHILLIPS, T.B., JACKSON, C.A.-L., BELL, R.E., DUFFY, O.B. & FOSSEN, H. (2016) Reactivation of intrabasement structures during rifting: A case study from offshore southern Norway. *Journal of Structural Geology*, **91**, 54–73. doi:10.1016/j.jsg.2016.08.008

REEMST, P. & CLOETINGH, S. (2000) Polyphase rift evolution of the Vøring margin (mid-Norway): Constraints from forward tectonostratigraphic modeling. *Tectonics*, **19** (2), 225–240. doi:10.1029/1999TC900025

REEVE, M.T., BELL, R.E. & JACKSON, C.A.-L. (2014) Origin and significance of intra-basement seismic reflections offshore western Norway. *Journal of the Geological Society*, **171** (1), 1. doi:10.1144/jgs2013-020

RIBER, L., DYPVIK, H. & SØRLIE, R. (2015) Altered basement rocks on the Utsira High and its surroundings, Norwegian North Sea. *NJG*. doi:10.17850/njg95-1-04

RO, H.E. & FALEIDE, J.I. (1992) A stretching model for the Oslo Rift. *Tectonophysics*, **208** (1), 19–36. doi:10.1016/0040-1951(92)90334-3

ROBERTS, A.M., YIELDING, G., KUSZNIR, N.J., WALKER, I. & DORN-LOPEZ, D. (1993) Mesozoic extension in the North Sea: constraints from flexural backstripping, forward modelling and fault populations. *Geological Society, London, Petroleum Geology Conference series*, **4** (1), 1123–1136. doi:10.1144/0041123

ROBERTS, A.M., YIELDING, G., KUZNIR, N.J., WALKER, I.M. & AND DORN-LOPES, D. (1995) Quantitative analysis of Triassic extension in the northern Viking Graben.

ROTEVATN, A., JACKSON, C.A.-L., TVEDT, A.B.M., BELL, R.E. & BLÆKKAN, I. (2019) How do normal faults grow? *Geol*, **125**, 174–184. doi:10.1016/j.jsg.2018.08.005

ROTEVATN, A., KRISTENSEN, T.B., KSIENZYK, A.K., WEMMER, K., HENSTRA, G.A., MIDTKANDAL, I., GRUNDVÅG, S.-A. & ANDRESEN, A. (2018) Structural Inheritance and Rapid Rift-Length Establishment in a Multiphase Rift: The East Greenland Rift System and its Caledonian Orogenic Ancestry. *Tectonics*, **37** (6), 1858–1875. doi:10.1029/2018TC005018

SALOMON, E., KOEHN, D. & PASSCHIER, C. (2015) Brittle reactivation of ductile shear zones in NW Namibia in relation to South Atlantic rifting. *Tectonics*, **34** (1), 70–85. doi:10.1002/2014TC003728

SCHULTZ, R.A., SOLIVA, R., FOSSEN, H., OKUBO, C.H. & REEVES, D.M. (2008) Dependence of displacement–length scaling relations for fractures and deformation bands on the volumetric changes across them. *Geol*, **30** (11), 1405–1411. doi:10.1016/j.jsg.2008.08.001

SCLATER, J.G. & CÉLÉRIER, B. (1988) Errors in extension measurements from planar faults observed on seismic reflection lines. *Basin Res*, **1** (4), 217–221. doi:10.1111/j.1365-2117.1988.tb00017.x

SÉRANNE, M. & SÉGURET, M. (1987) The Devonian basins of western Norway: tectonics and kinematics of an extending crust. *Geological Society, London, Special Publications*, **28** (1), 537. doi:10.1144/GSL.SP.1987.028.01.35

SLAGSTAD, T., DAVIDSEN, B. & DALY, J.S. (2011) Age and composition of crystalline basement rocks on the Norwegian continental margin: offshore extension and continuity of the Caledonian–Appalachian orogenic belt. *Journal of the Geological Society*, **168** (5), 1167–1185. doi:10.1144/0016-76492010-136

SØMME, T.O., MARTINSEN, O.J. & LUNT, I. (2013) Linking offshore stratigraphy to onshore paleotopography: The Late Jurassic–Paleocene evolution of the south Norwegian margin. *GSA Bulletin*, **125** (7-8), 1164–1186. doi:10.1130/B30747.1

STEEL, R. & RYSETH, A. (1990) The Triassic — early Jurassic succession in the northern North Sea: megasequence stratigraphy and intra-Triassic tectonics. *Geological Society, London, Special Publications*, **55** (1), 139. doi:10.1144/GSL.SP.1990.055.01.07

STEEL, R.J. (1993) Triassic–Jurassic megasequence stratigraphy in the Northern North Sea: rift to post-rift evolution. *Petroleum Geology Conference series*, **4** (1), 299. doi:10.1144/0040299

SVARTMAN DIAS, A.E., LAVIER, L.L. & HAYMAN, N.W. (2015) Conjugate rifted margins width and asymmetry: The interplay between lithospheric strength and thermomechanical processes. *J. Geophys. Res. Solid Earth*, **120** (12), 8672–8700. doi:10.1002/2015JB012074

TER VOORDE, M, FÆRSETH, R.B., GABRIELSEN, R. H. & CLOETINGH, S. A. P. L. (2000) Repeated lithosphere extension in the northern Viking Graben: a coupled or a decoupled rheology?

TETREAULT, J.L. & BUITER, S.J.H. (2018) The influence of extension rate and crustal rheology on the evolution of passive margins from rifting to break-up. *Tectonophysics*, **746**, 155–172. doi:10.1016/j.tecto.2017.08.029

TETT, D.L. & SAWYER, D.S. Dynamic models of the multiphase continental rifting and their implications for the Newfoundland and Iberia conjugate margins., (149), 635–647.

TOMASSO, M., UNDERHILL, J.R., HODGKINSON, R.A. & YOUNG, M.J. (2008) Structural styles and depositional architecture in the Triassic of the Ninian and Alwyn North fields: Implications for basin development and prospectivity in the Northern North Sea. *Marine and Petroleum Geology*, **25** (7), 588–605. doi:10.1016/j.marpetgeo.2007.11.007

UNDERHILL, J.R. & PARTINGTON, M.A. (1993) Jurassic thermal doming and deflation in the North Sea: implications of the sequence stratigraphic evidence. *Petroleum Geology Conference series*, **4** (1), 337. doi:10.1144/0040337

VAN WIJK, J.W. & CLOETINGH, S.A.P.L. (2002) Basin migration caused by slow lithospheric extension. *Earth and Planetary Science Letters*, **198** (3), 275–288. doi:10.1016/S0012-821X(02)00560-5

VEEN, J.H. ten & KLEINSPEHN, K.L. (2000) Quantifying the timing and sense of fault dip slip: New application of biostratigraphy and geohistory analysis. *Geology*, **28** (5), 471–474. doi:10.1130/0091-7613(2000)28<471:QTTASO>2.0.CO;2

VETTI, V.V. & FOSSEN, H. (2012) Origin of contrasting Devonian supradetachment basin types in the Scandinavian Caledonides. *Geology*, **40** (6), 571–574. doi:10.1130/G32512.1

WALSH, J., WATTERSON, J. & YIELDING, G. (1991) The importance of small-scale faulting in regional extension. *Nature*, **351** (6325), 391–393. doi:10.1038/351391a0

WELFORD, J.K., SMITH, J.A., HALL, J., DEEMER, S., SRIVASTAVA, S.P. & SIBUET, J.-C. (2010) Structure and rifting evolution of the northern Newfoundland Basin from Erable multichannel seismic reflection profiles across the southeastern margin of Flemish Cap. *Geophys J Int*, **180** (3), 976–998. doi:10.1111/j.1365-246X.2009.04477.x

997 WHIPP, P.S., JACKSON, C.A.-L., GAWTHORPE, R.L., DREYER, T. & QUINN, D. (2014) Normal fault array
998 evolution above a reactivated rift fabric; a subsurface example from the northern Horda
999 Platform, Norwegian North Sea. *Basin Res*, **26** (4), 523–549. doi:10.1111/bre.12050
1000 WRONA, T., MAGEE, C., FOSSEN, H., GAWTHORPE, R.L., BELL, R.E., JACKSON, C.A.-L. & FALEIDE, J.I. (2019) 3-D
1001 seismic images of an extensive igneous sill in the lower crust. *Geology*, **47** (8), 729–733.
1002 doi:10.1130/G46150.1
1003 ZIEGLER, P.A. (1990) Tectonic and palaeogeographic development of the North Sea rift system.
1004 *Tectonic Evolution of North Sea Rifts*, 1–36.
1005 ZIEGLER, P.A. (1992) North Sea rift system. *Tectonophysics*, **208** (1), 55–75. doi:10.1016/0040-
1006 1951(92)90336-5
1007

Figure 1

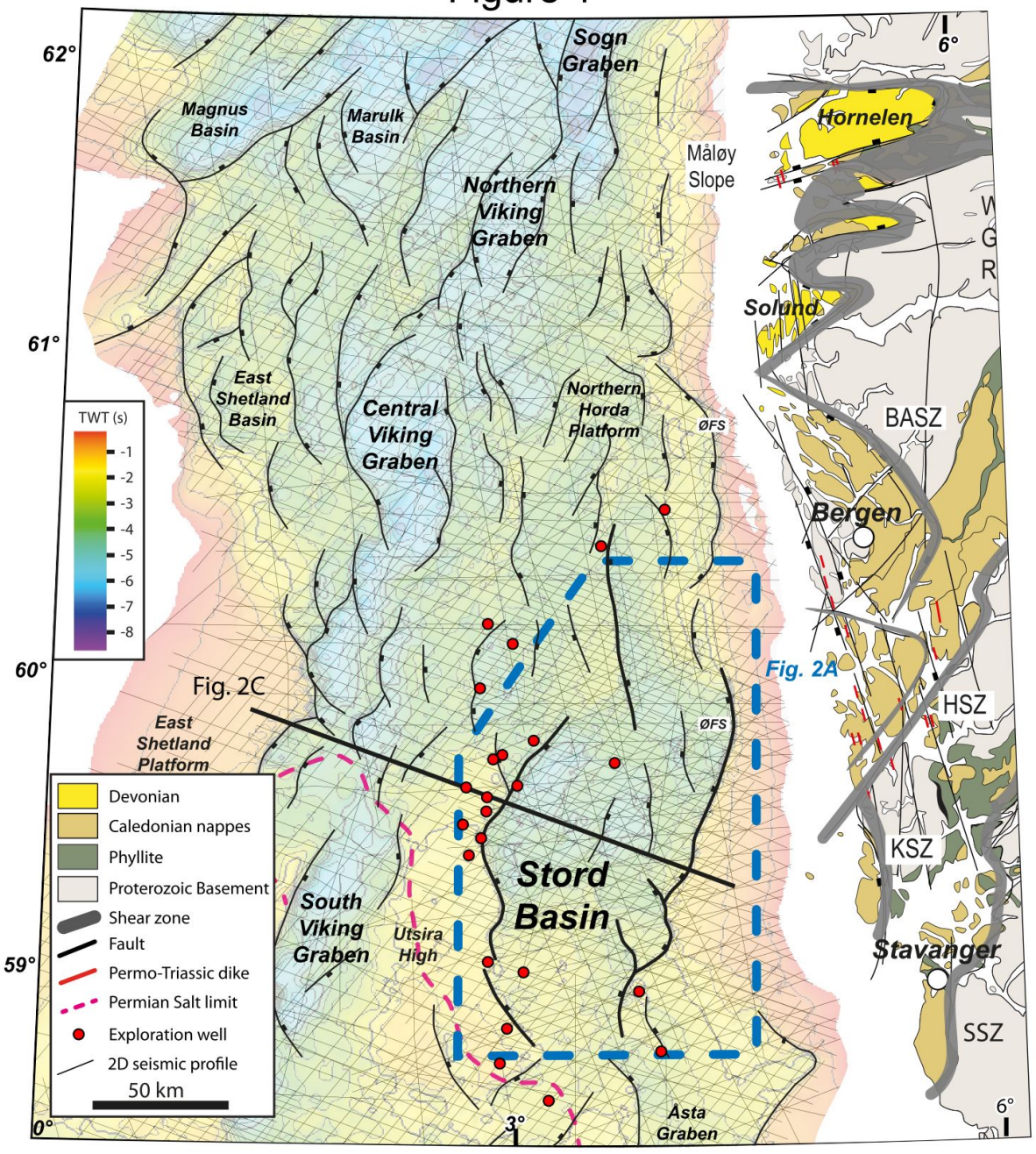

1008

Figure 2

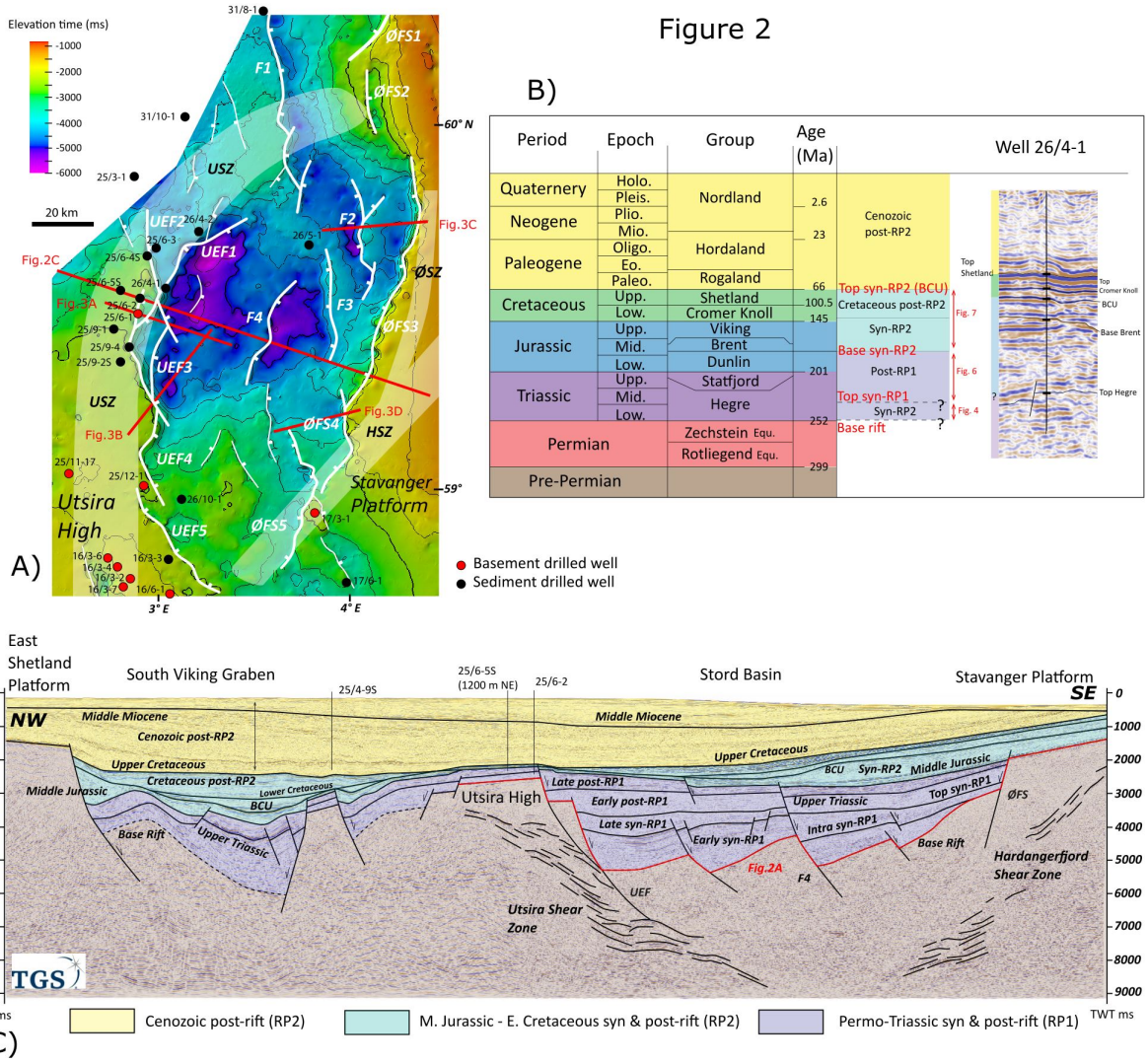
A)
Elevation time (ms)
-1000
-2000
-3000
-4000
-5000
-6000
20 km
31/8-1
31/10-1
25/3-1
25/6-3
26/4-2
25/6-4S
26/4-1
25/6-5S
25/6-2
25/6-1
25/9-1
25/9-4
25/9-2S
25/11-17
25/12-11
26/10-1
16/3-6
16/3-4
16/3-2
16/3-7
16/6-1
17/3-1
17/6-1
26/5-1
ØFS1
ØFS2
ØFS3
ØFS4
ØFS5
F1
F2
F3
F4
USZ
UEF1
UEF2
UEF3
UEF4
UEF5
ØSZ
HSZ
Fig.2C
Fig.3A
Fig.3B
Fig.3C
Fig.3D
Utsira High
Stavanger Platform
60° N
59°
3° E
4° E
Basement drilled well
Sediment drilled well
B)
Period
Epoch
Group
Age (Ma)
Well 26/4-1
Quaternery
Holo.
Pleis.
Nordland
2.6
Neogene
Plio.
Mio.
23
Hordaland
Paleogene
Oligo.
Eo.
Paleo.
Rogaland
66
Cretaceous
Upp.
Low.
Shetland
Cromer Knoll
100.5
145
Jurassic
Upp.
Mid.
Low.
Viking
Brent
Dunlin
201
Triassic
Upp.
Mid.
Low.
Statfjord
Hegre
252
Permian
Zechstein Equ.
Rotliegend Equ.
299
Pre-Permian
Cenozoic post-RP2
Top syn-RP2 (BCU)
Cretaceous post-RP2
Syn-RP2
Base syn-RP2
Post-RP1
Top syn-RP1
Syn-RP2
Base rift
Fig. 7
Fig. 6
Fig. 4
Top Shetland
Top Cromer Knoll
BCU
Base Brent
Top Hegre
C)
East Shetland Platform
South Viking Graben
25/4-9S
25/6-5S (1200 m NE)
25/6-2
Stord Basin
Stavanger Platform
NW
SE
Middle Miocene
Cenozoic post-RP2
Upper Cretaceous
Cretaceous post-RP2
Middle Jurassic
Lower Cretaceous
BCU
Base Rift
Upper Triassic
Utsira High
Late post-RP1
Early post-RP1
Late syn-RP1
Early syn-RP1
Upper Cretaceous
BCU
Syn-RP2
Middle Jurassic
Top syn-RP1
Upper Triassic
Intra syn-RP1
Base Rift
ØFS
Hardangerfjord Shear Zone
Fig.2A
F4
UEF
Utsira Shear Zone
TGS
0
1000
2000
3000
4000
5000
6000
7000
8000
9000
TWT ms
Cenozoic post-rift (RP2)
M. Jurassic - E. Cretaceous syn & post-rift (RP2)
Permo-Triassic syn & post-rift (RP1)

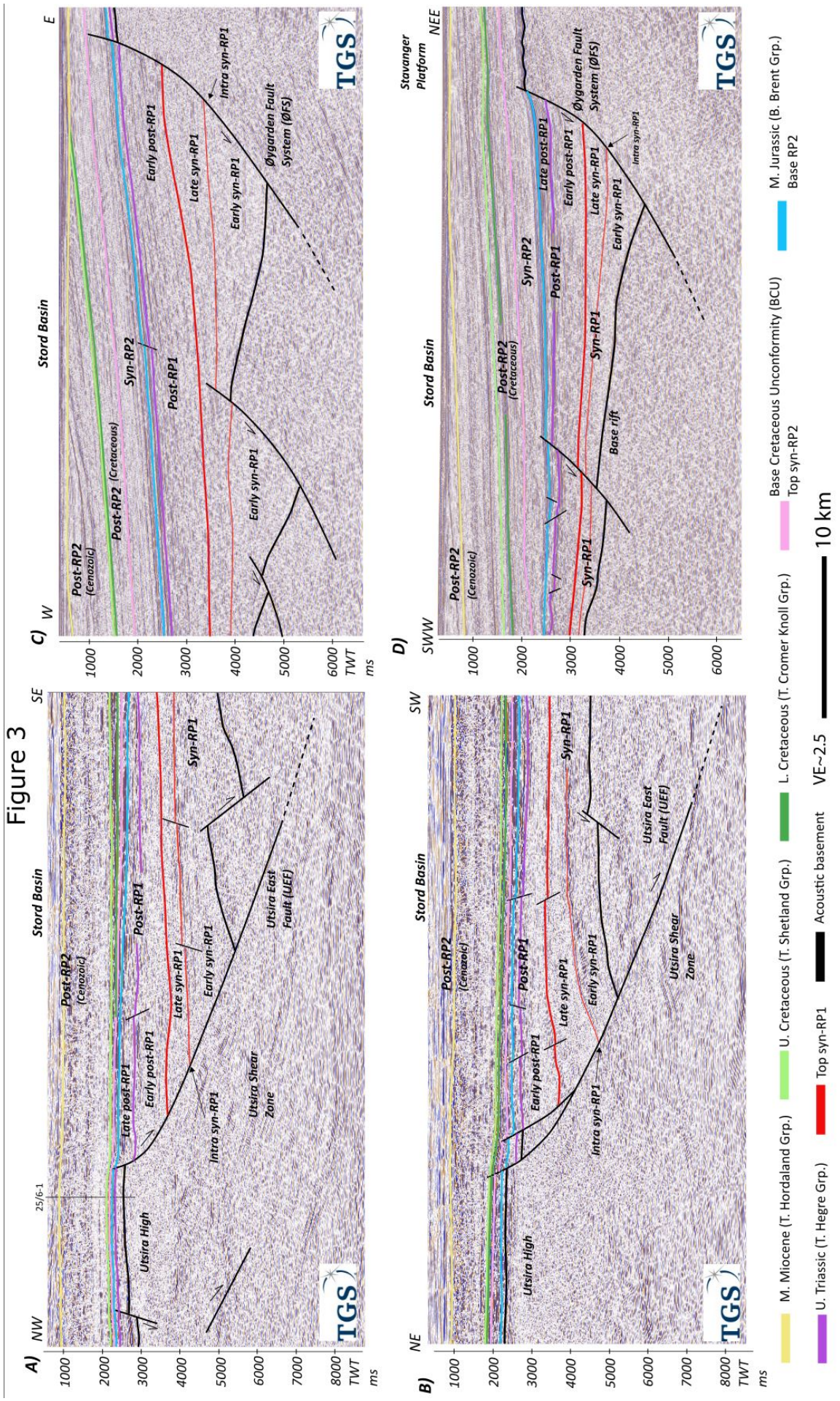

Figure 3

1012

Figure 4

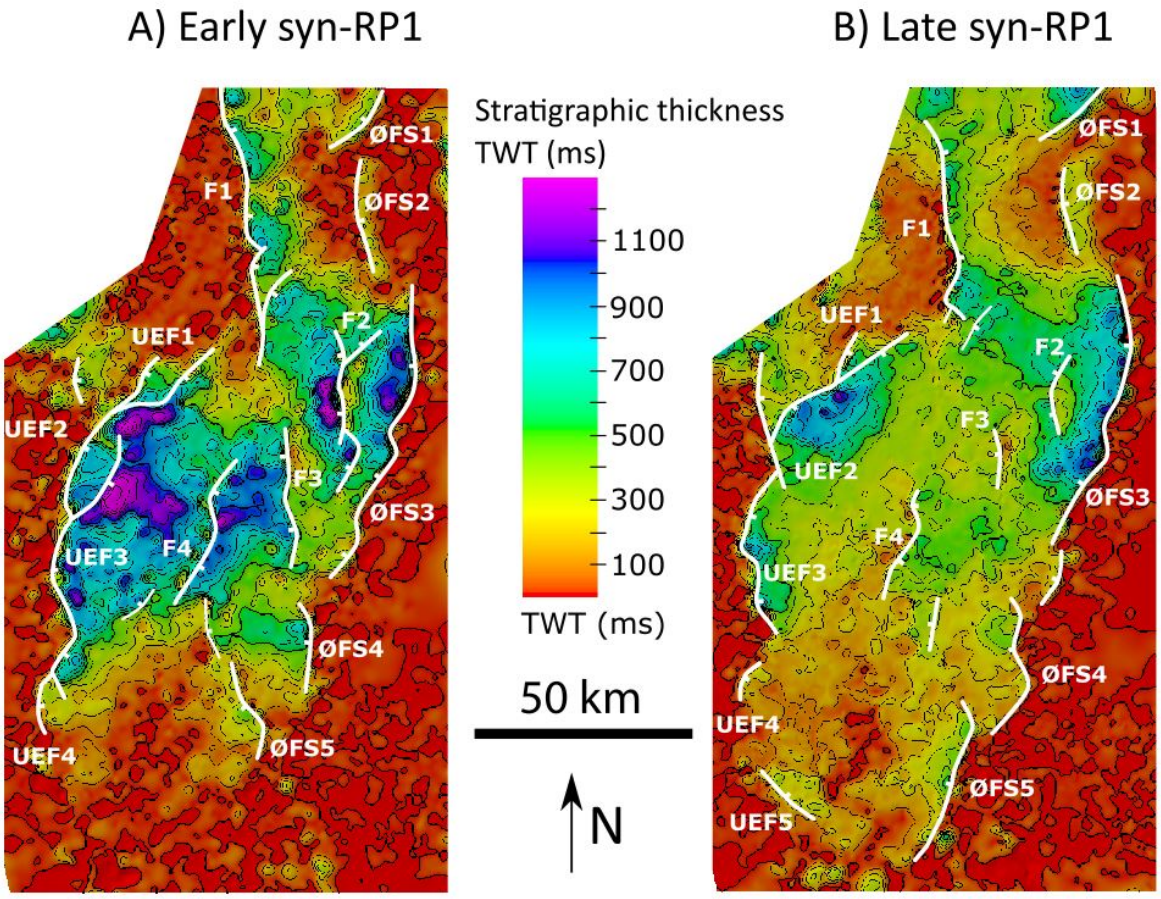

Figure 5

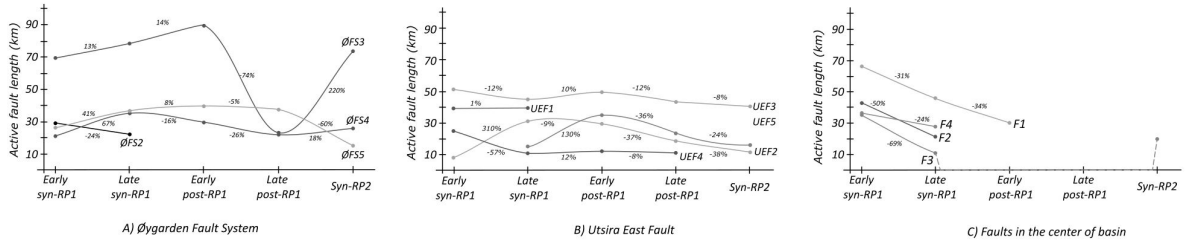

Figure 6

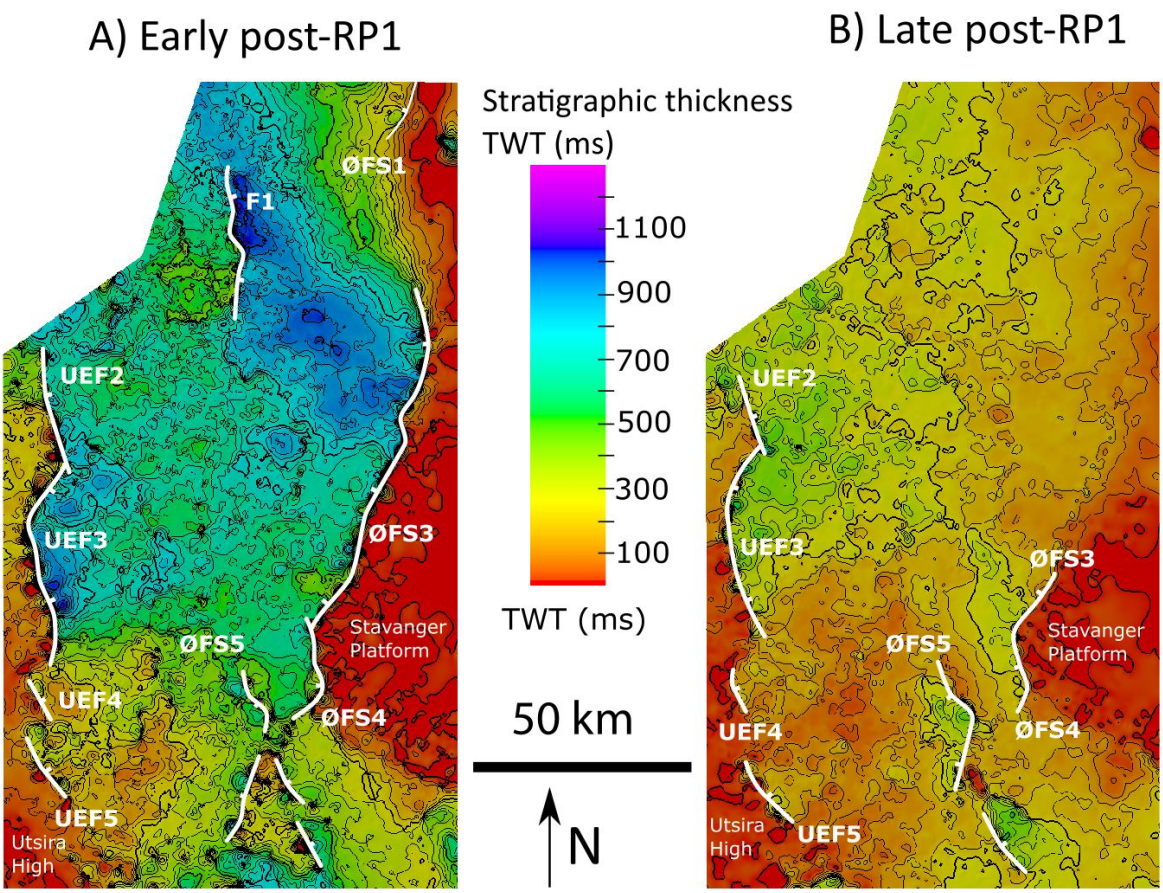

1020

1021

1022

Figure 7

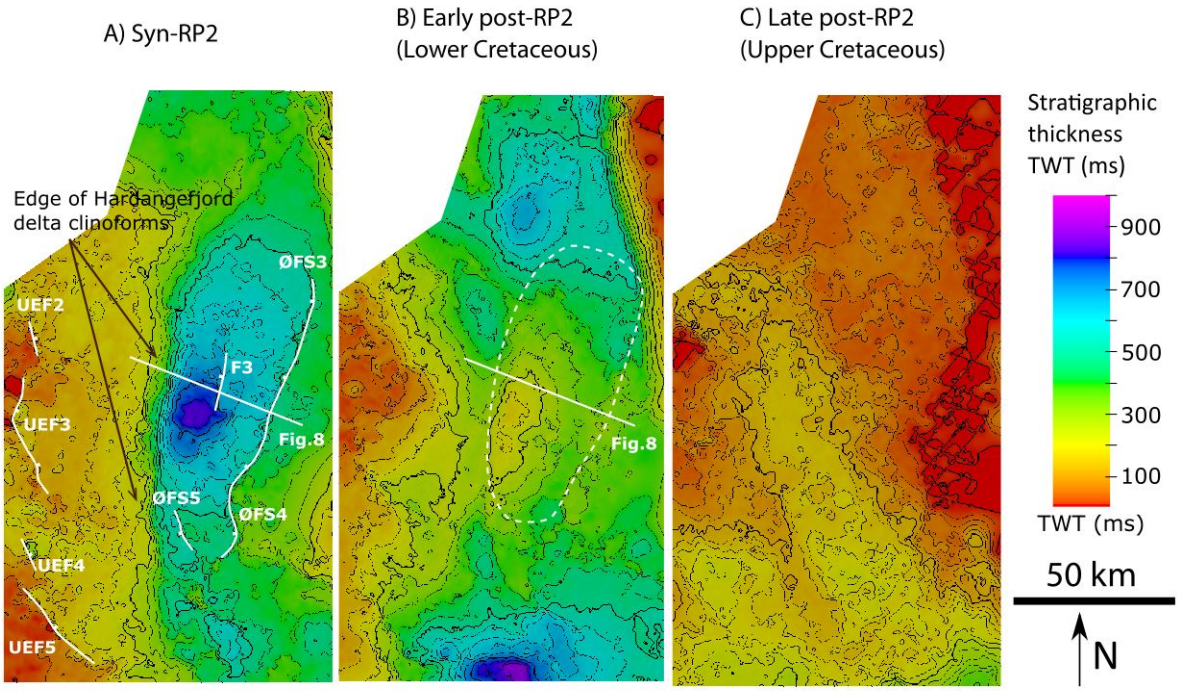

1023

1024

1025

1026

1027

Figure 8

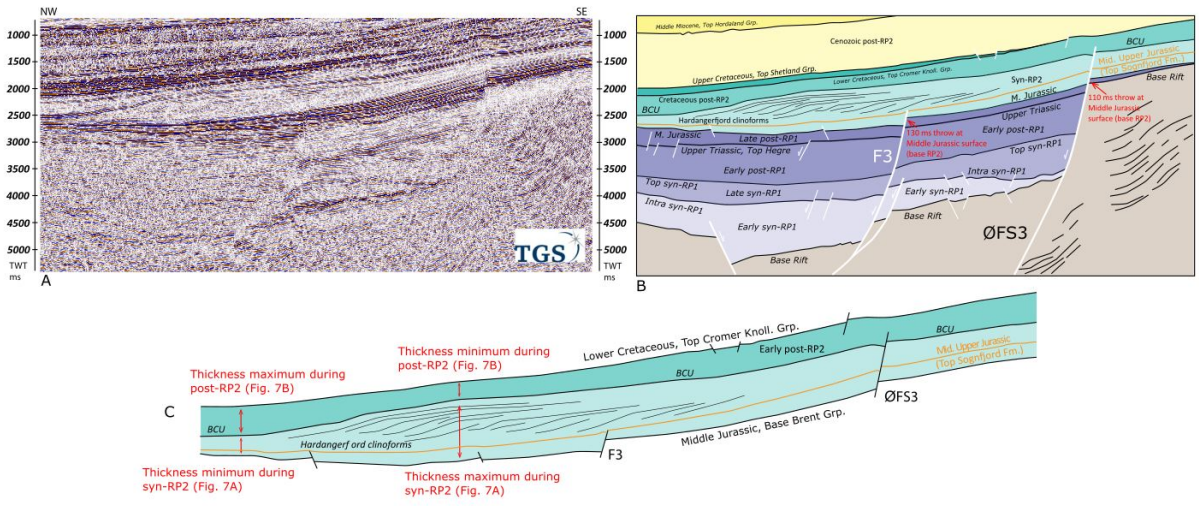

1028

Figure 9

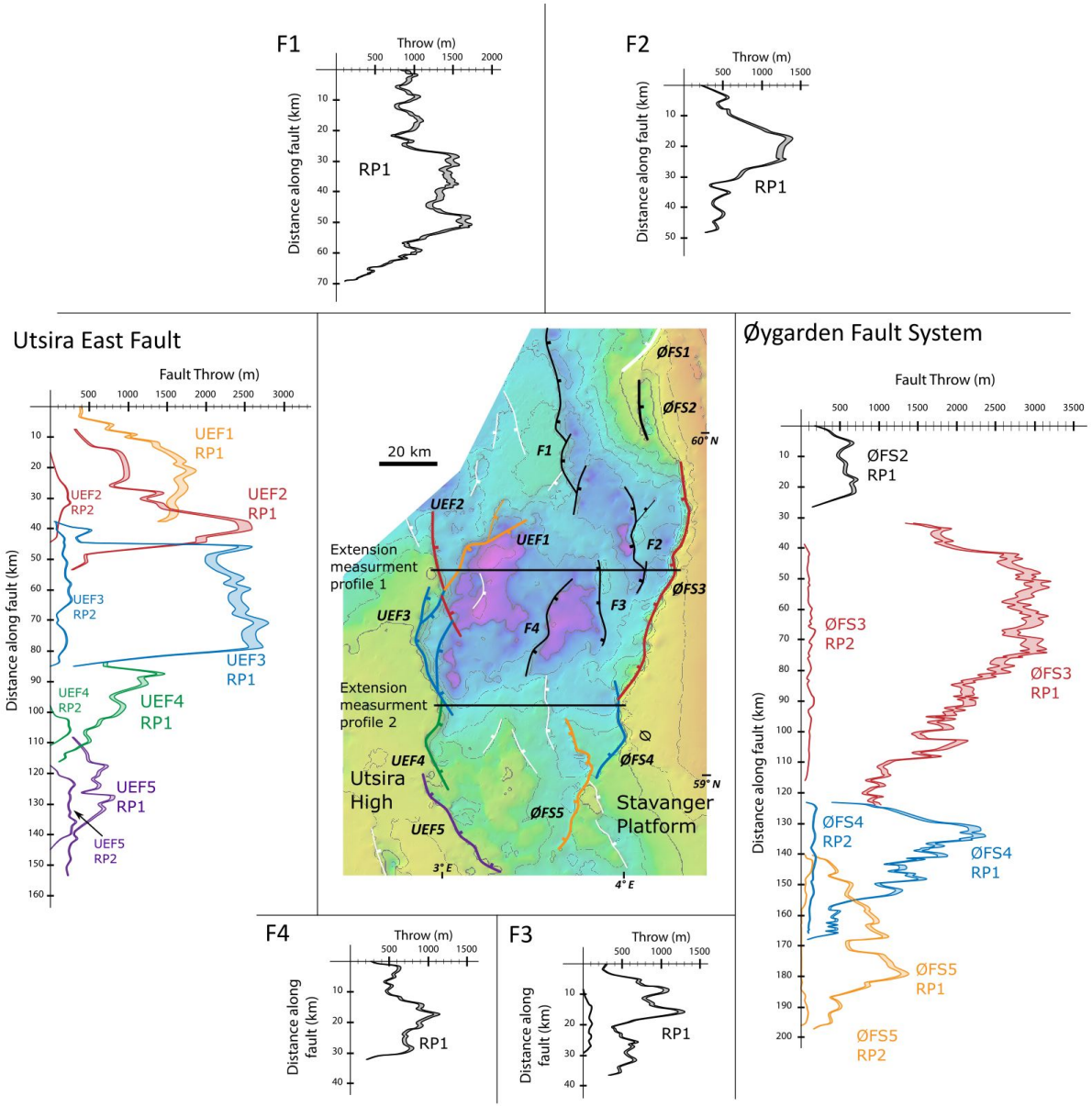

1029

Figure 10

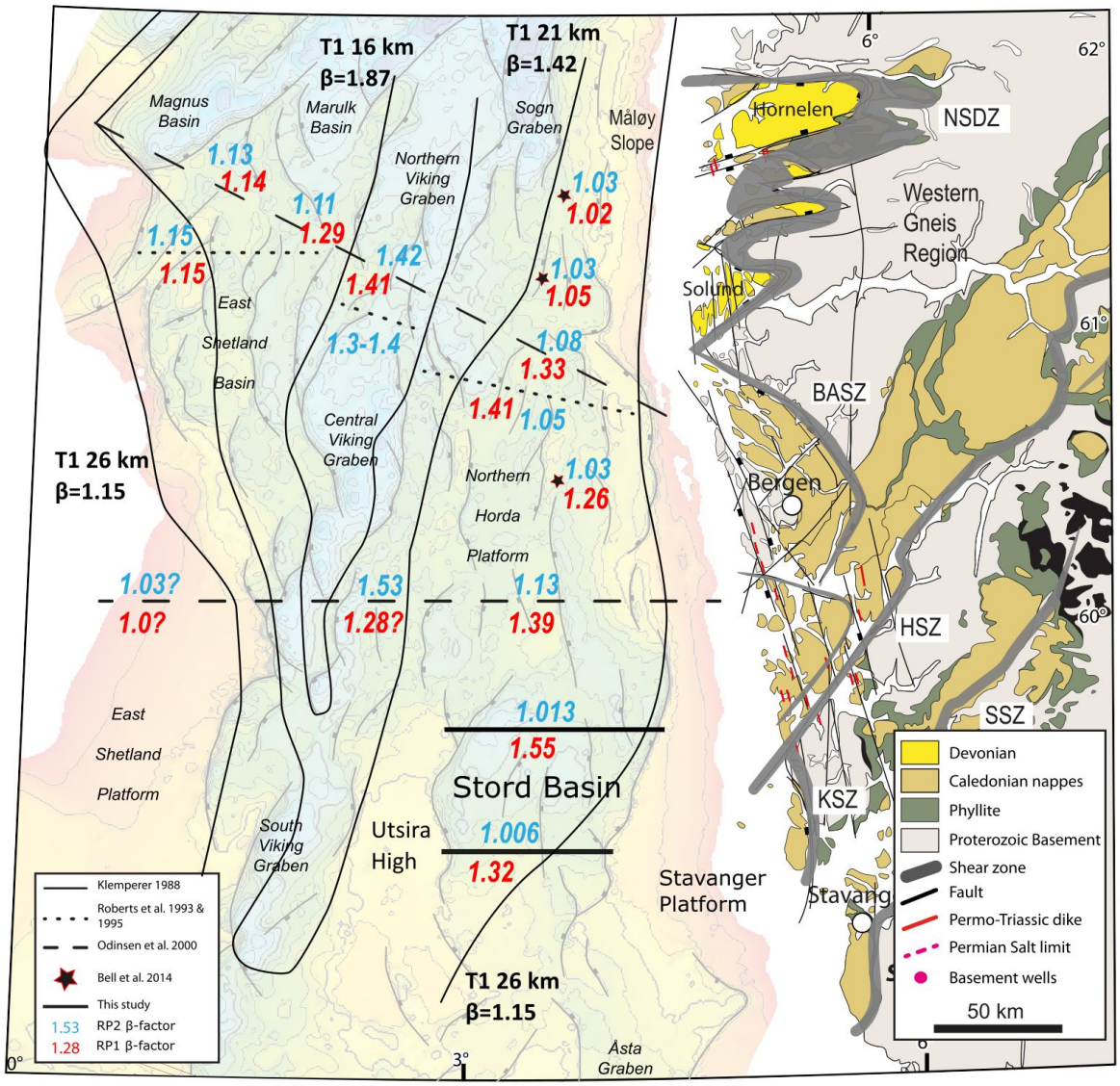

1030

Figure 11

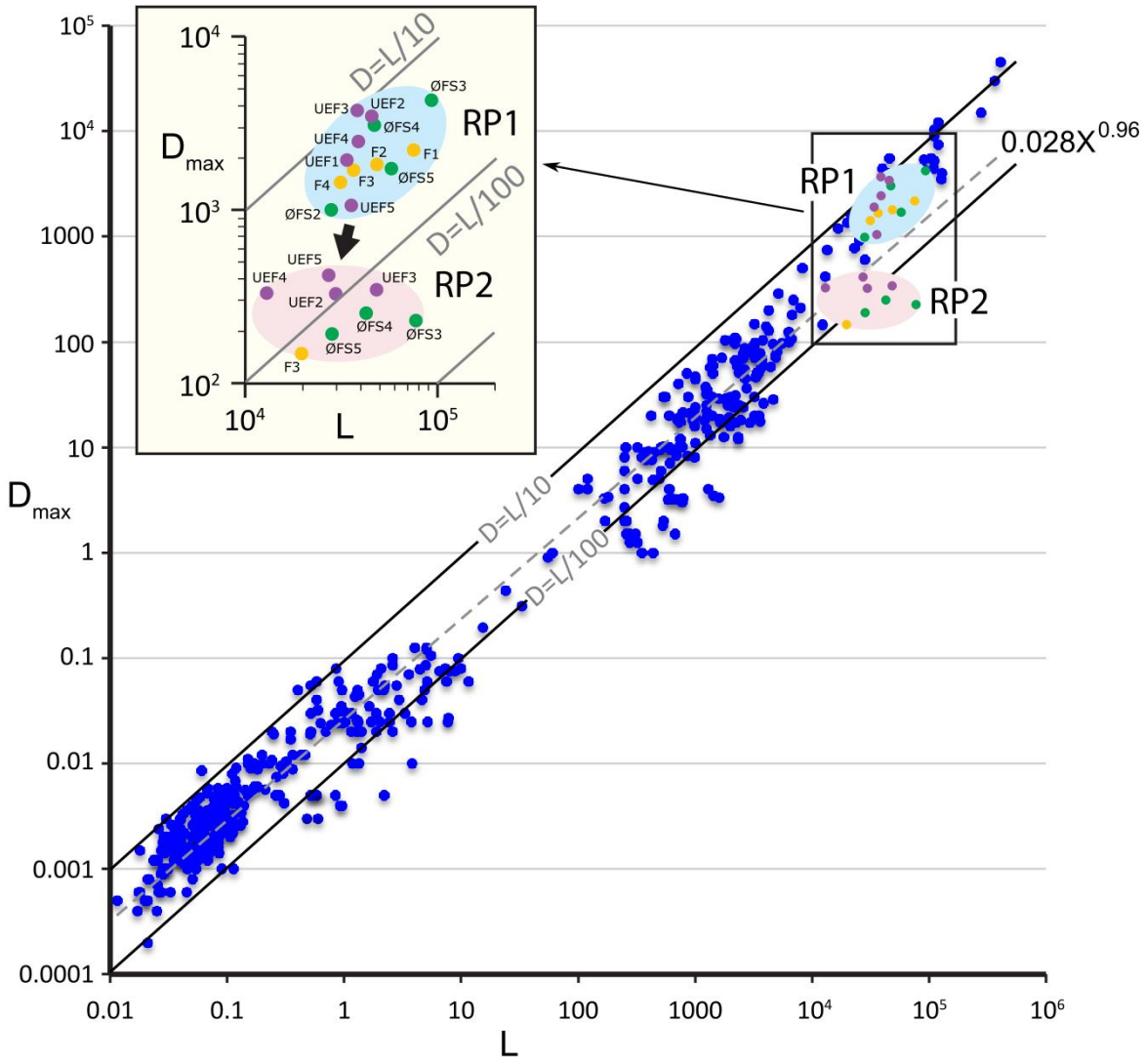

1031

Table 1

	Northern Stord Basin		Southern Stord Basin	
	RP1	RP2	RP1	RP2
Profile length, T1 (km)	83.55	84.30	61.20	61.45
Measured heave	23.30	0.75	11.20	0.25
Initial profile length, T0 (km)	60.25	83.55	50	61.20
Calculated β	1.39	1.009	1.22	1.004
Corrected for subseismic faulting (30%)	1.55	1.013	1.32	0.006

1032

1033

1034

1035

Appendix 1

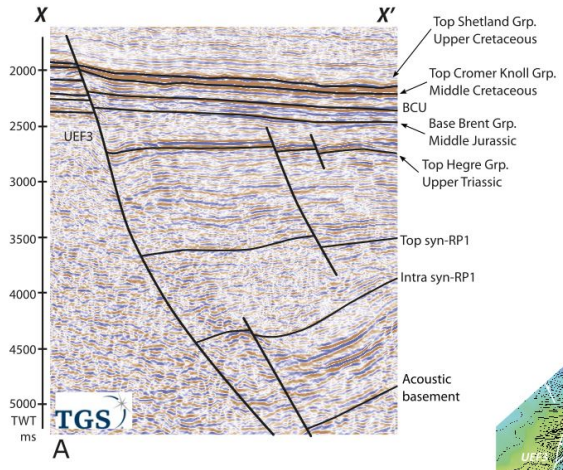

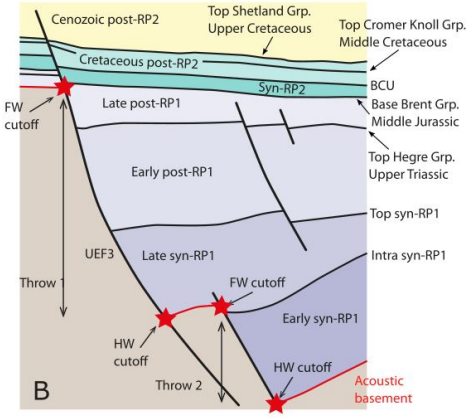

Cumulative throw = throw 1 + throw 2

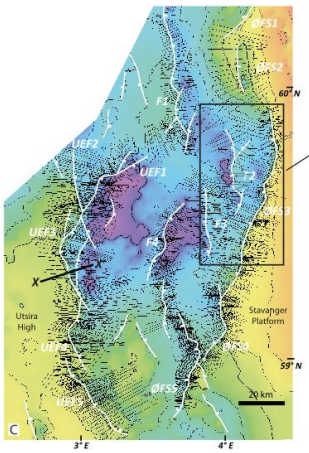

C: Time-structure map at base RP1 showing created synthetic sections

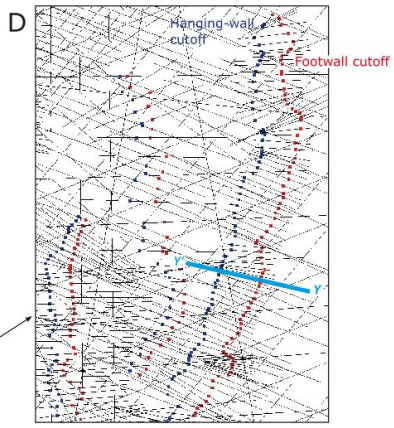

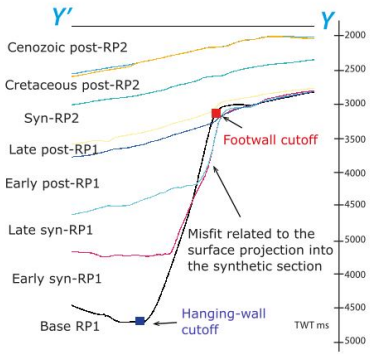

E: Synthetic section across ØFS3

1036

1037

Appendix 2

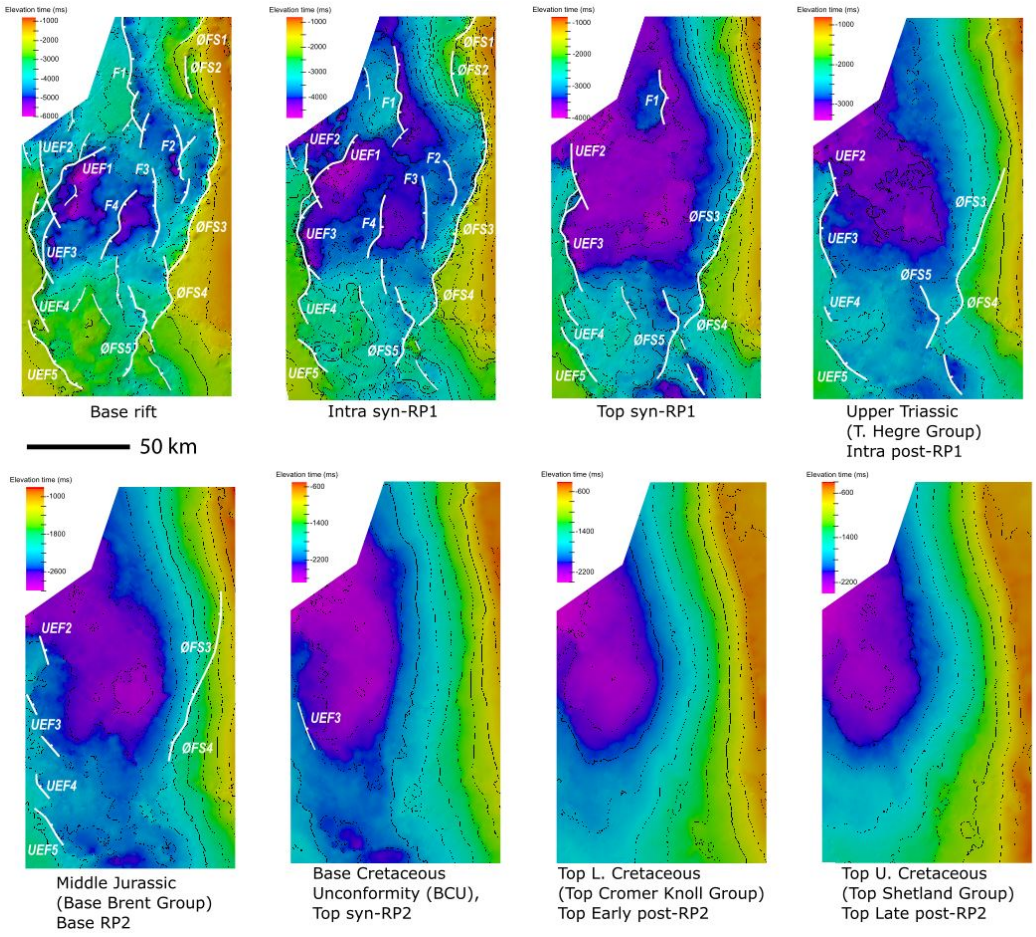

1038